Tectonophysics 663 (2015) 419–433

Contents lists available at ScienceDirect

Tectonophysics

journal homepage: www.elsevier.com/locate/tecto

Crust and mantle lithospheric structure of the Iberian Peninsula deduced from potential field modeling and thermal analysis

Montserrat Torne [a,*], Manel Fernàndez [a], Jaume Vergés [a], Conxi Ayala [b,1], Maria Carolina Salas [c], Ivone Jimenez-Munt [a], Grant George Buffett [a], Jordi Díaz [a]

[a] Institute of Earth Sciences Jaume Almera, ICTJA–CSIC, Lluis Solé i Sabarís s/n, 08028 Barcelona, Spain
[b] Instituto Geológico y Minero de España—IGME, La Calera n. 1, 28760 Tres Cantos, Madrid, Spain
[c] Universidad Simón Bolivar, Caracas, Venezuela

ARTICLE INFO

Article history:
Received 9 December 2014
Received in revised form 29 April 2015
Accepted 2 June 2015
Available online 12 June 2015

Keywords:
Elevation
Geoid anomaly
3D gravity modeling
Residual gravity anomalies
Crustal and lithospheric structure
Iberian Peninsula

ABSTRACT

We investigate the lithospheric structure of the Iberian Peninsula and lateral crustal density variations using a three-step approach. First the crustal and mantle lithosphere thicknesses are calculated from joint geoid and elevation modeling combined with thermal analysis further constrained by seismic data. We then compute the 3D gravity effect of the resulting lithospheric structure to separate the measured Bouguer anomaly into its regional and local components. Finally we invert the residual gravity anomalies to highlight lateral average crustal density variations and discuss them in terms of crustal structures. Our results show that for the majority of the study area the crustal thickness does correlate with the regional topography pattern. The highest topography – above 1500 m – shows thicknesses above 44 km with local values up to 48 km. Crustal thicknesses in the range of 36–40 km are obtained in the uplifted Alpine areas while a thinner crust is observed in sedimentary basins and in the Iberian Massif (30 to 35 km) with the exception of SW Iberia region where the crust thins from 30 to 28 km. Thick lithosphere – above 140 km – is found along the Pyrenees, the Cantabrian Mountains, the Iberian Chain and in the Betics while the thinnest lithosphere is found in SW Iberia (90 km). 3D inversion of residual anomalies show that for the majority of the area the average density of the crust is in the range of 2810 ± 10 kg m^{-3}. The denser crust is found in the NW and SW regions of the Iberian Massif (+30 kg m^{-3} on average) and locally in the Pyrenees (above +70 kg m^{-3}), NW of the Iberian Chain (+15 kg m^{-3} on average) and in the southern Internal Betics (+70 kg m^{-3}). The least dense crust is found in the central and western Betic Chain (−30 kg m^{-3} on average) and in sedimentary basin depocenters.

1. Introduction

The Iberian Peninsula, is located at the westernmost end of the Alpine-Himalayan belt (Fig. 1) having formed as a result of the Tertiary closure of the Tethys Ocean during the collision of India, Arabia and Africa with Eurasia (Dercourt et al., 1986). Its lithospheric configuration is the result of four main tectonic cycles that have left their imprint on its present-day geometry and compositional signature. These are: (i) the Variscan orogeny giving rise to the Variscan mountain belt extending from Asia to North Africa, (ii) the subsequent Mesozoic dismembering of the majority of Variscan terrains occurring during the Permo-Triassic and the Late Jurassic–Early Cretaceous, which resulted in the opening of numerous extensional Mesozoic basins with different orientations, (iii) the Alpine orogeny, lasting from Late Cretaceous (chron 33, 80 Ma) to recent that caused the inversion of the extended Mesozoic basins and the build-up of orogenic belts along the northern and southern plate boundaries amid severe intraplate deformation and (iv) the coeval extension and compression on its eastern and southern boundaries that resulted in the opening of the western Mediterranean during the Neogene–Quaternary.

Continental collision between Laurasia and Gondwana (Variscan orogeny) occurred from Late Devonian, ca 370 Ma, and Carboniferous, ca 290 Ma, and gave rise to a 12,000 km long mountain belt extending from Asia to the north and northwest of Africa (Martínez-Catalán et al., 2009). The European segment, with a length of about 3000 km and a width in the range of 700 to 900 km, extended from the Iberian Peninsula to the North of Bohemia (Pérez-Estaún et al., 2004). This collisional episode could have resulted in crustal density variations and possibly mantle depletion during the Late Paleozoic. A large areal extent of Carboniferous volcanic rocks recorded along the Rheno-Hercynian foreland fold and thrust belt, e.g. South Portugal, the abundance of granitoids, and the exhumation of HT/LP metamorphic rocks

* Corresponding author at. Institute of Earth Sciences Jaume Almera, ICTJA-CSIC, Lluis Solé i Sabarís s/n, E08028 Barcelona, Spain.
E-mail address: montserrat.torne@ictja.csic.es (M. Torne).
[1] Now visiting at the Institute of Earth Sciences Jaume Almera–CSIC, Lluis Solé i Sabarís s/n, 08028 Barcelona, Spain.

http://dx.doi.org/10.1016/j.tecto.2015.06.003
0040-1951/

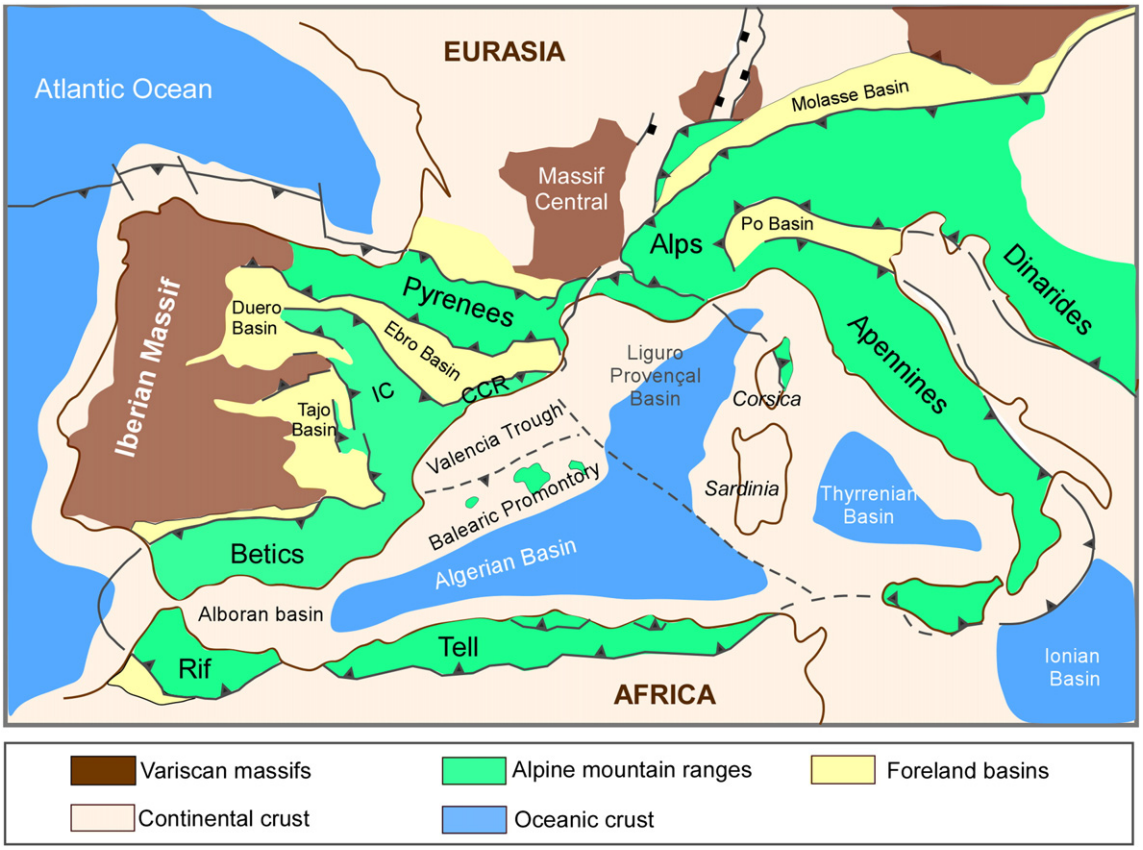

Fig. 1. Map of the Western Alpine–Himalayan collisional belt with locations of main orogenic chains related to the Africa–Europe collision indicated (based on Vergés and Sabat, 1999). The Iberian Peninsula is located at the westernmost limit of the approximately 12,000 km long Alpine–Himalayan Belt. IC, Iberian Chain; CCR, Catalan Coastal Ranges.

show widespread heating and thermal weakening of the crust. This may indicate that in early Carboniferous times the Variscan crust and lithosphere were hot and, following Franke (2014), likely of moderate thickness.

From Late Permian to Middle Jurassic, the widespread Mesozoic tensional regime gave rise to a multidirectional continental rift system that transected the Variscan belt, its European foreland and the North Atlantic area, culminating in crustal break-up along the Atlantic margin (e.g., Ziegler, 1992). On the Iberian Peninsula, this episode resulted in the formation of extensional basins with different orientations located on its northern and southern borders as well as in the interior of the plate. As pointed out by Vergés and Fernàndez (2006), the Mesozoic extension led to the separation of about 125 to 150 km between the central and eastern sides of France and Spain and at least 35 km in the former Iberian realm. On its southern border, recent plate reconstructions indicate that the average separation between the African and Iberian mainlands was about 350–450 km in a NW–SE direction (Vergés and Fernàndez, 2012).

The Alpine collision from Late Cretaceous (chron 33, 80 Ma) to Oligocene resulted in: i) the uplift of orogenic belts along its northern plate boundary, ii) significant intraplate deformation, iii) the formation of the large Tertiary basins close to these bounding mountain chains, and iv) inversion of some Variscan structures (Figs. 1 and 2).

From the end of the Oligocene (24 Ma) to the Quaternary, coeval extension and compression gave rise to the formation of the westernmost Mediterranean basins (Liguro-Provençal, Valencia Trough, Algeria, and Alboran basins) and the surrounding orogenic systems (Catalan Coastal Ranges and Betic-Rif-Tell system) (Fig. 1 and 2).

Thus, the Iberian Peninsula displays a complex structure with Variscan terrains outcropping at its western side, the so called Iberian Massif variably deformed during the Alpine orogeny; inter and intraplate Alpine mountain ranges of diverse structural trends; their bounding sedimentary basins; and the Neogene extensional basins located along its eastern and southern Mediterranean margins (Fig. 1). As a result of this complex tectonic evolution, conspicuous lateral variations in both crustal and mantle lithosphere thickness, as well as in lithological composition, are expected.

The base of the crust is well constrained from Deep Seismic Sounding (DSS) models (Díaz and Gallart, 2009) and Receiver Function (RF) analysis (Mancilla and Díaz). Unlike the base of the crust, the base of the lithosphere for the whole Iberian Peninsula is poorly known. The main information comes from 2D lithospheric modeling along three profiles crossing the entire peninsula from N to S (Carballo et al., 2015a-in this volume); and its NE (Carballo et al., 2015b) and SW regions (Fernàndez et al., 2004; Palomeras et al., 2011). Additional information comes from 3D modeling of its southern regions (Fullea et al., 2010 and Torne et al., 2000) and from tomography studies (e.g., Bezada et al., 2013; Bonnin et al., 2014; Chevrot et al., 2014; Díaz et al., 2013; Palomeras et al., 2014).

The main goal of this work is to advance the knowledge on the 3D crustal and mantle structure of the entire Iberian Peninsula. To that end, we employ a three-step approach. First we map the crustal and mantle lithosphere thicknesses by joint modeling elevation and geoid anomaly data together with thermal analysis that is further constrained by Moho depths obtained from DSS experiments and RF analysis. Second, we compute the 3D gravity effect of the obtained lithospheric structure (the crust and mantle lithospheric thickness) and subtract it from the measured Bouguer anomaly to separate its regional and local components. Third we invert the obtained residual gravity anomalies to highlight lateral average crustal density variations and discuss them in terms of geological domains and crustal structures.

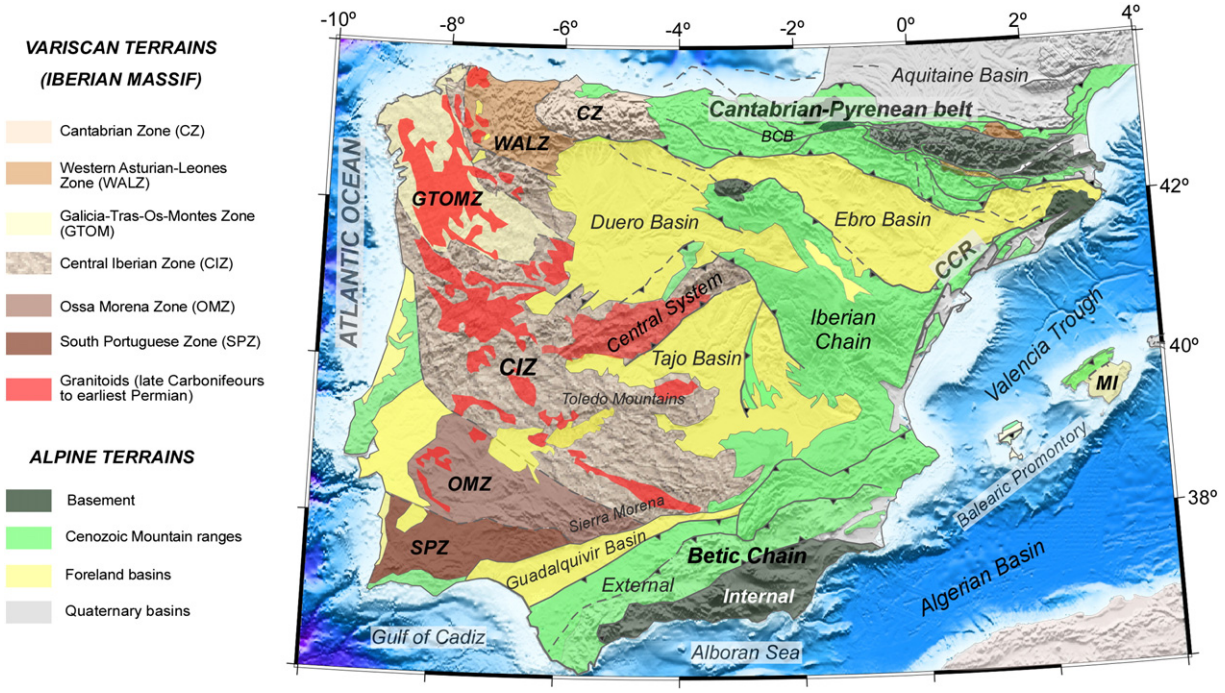

Fig. 2. Tectonic map of the Iberian Peninsula based on Rodríguez-Fernández (2004) and the tectonic map of the Pyrenees of Vergés et al. (1995). Location of granitoids along the Iberian Massif has been taken from Simancas et al (2013). Iberian Massif: CZ, Cantabrian Zone; WALZ, Western Asturian–Leonese Zone; CIZ, Central Iberian Zone; GTMOZ, Galicia-Tras-os-Montes Zone; OMZ, Ossa-Morena Zone and SPZ, South Portuguese Zone. Alpine mountain ranges: Cantabrian–Pyrenean belt; Betic Chain; Central System; Iberian Chain; CCR, Catalan Coastal Ranges. Foreland basins: Ebro, Duero, Tajo, and Guadalquivir basins. Neogene extended basins: Valencia Trough, Algerian and Alboran basins. BCB, Basque–Cantabrian Basin; MI, Mallorca Island.

2. Geological setting

For the purpose of this study we divide the rocks that outcrop in the Iberian Peninsula into two principal domains: Variscan and Alpine, which will facilitate highlighting results of their crustal and lithospheric structures.

The *Variscan domain* is composed of terrains of Upper Precambrian to Lower Permian age. It forms the basement of the Iberian Peninsula and crops out in Western and Central Iberia in the Iberian Massif, in the axial zone of the Pyrenees and in the interior of the Betics. Locally, some outcrops can also be traced in the Iberian and Catalan Coastal ranges and on the island of Menorca (Fig. 2).

The Iberian Massif constitutes the most complete exposure of the European Variscan orogen since it offers a complete section of an old collisional orogen (Martínez-Catalán et al., 2009). The Iberian Massif, together with the Armorican Massif (northwestern France), shows a marked bend known as the Ibero-Armorican Arc. It is divided into six zones parallel and concentric to the Arc that from north to south are: the Cantabrian Zone, located in the center of the Arc, the West Asturian–Leonese Zone, the Central Iberian Zone, the Galicia-Tras-os-Montes Zone, and the Ossa-Morena and South Portuguese zones (Julivert et al., 1972; Martínez-Catalán, 2011; Pérez-Estaún et al., 2004) (Fig. 2).

Pérez-Estaún et al. (1988, 2004) documented that the belt had double vergence; while the Cantabrian Zone and South Portuguese Zone (located to the north and south of the Massif) show typical characteristics of the outer zones of a mountain range – abundant synorogenic sediments and thin-skinned tectonics – the rest of the zones display internal domain characteristics (e.g. significant deformation, magmatism and metamorphism).

The *Alpine domain* is characterized at upper crustal levels by tectonic units with Mesozoic to recent deposits. It comprises: (i) the mountain belts located at the northern and southern boundaries of the Iberian Plate (the E–W oriented Pyrenean–Cantabrian belt to the north and the ENE–WSW oriented Betic Chain to the south); (ii) the NW–SE trending intraplate Iberian Chain and the NE–SW trending Catalan Coastal Ranges, both located at the NE side of Iberia; and (iii) the large Cenozoic foreland basins filled up by thick sedimentary sequences, that from north to south are: the Ebro, Tajo and Guadalquivir basins (Fig. 2). Some small post-orogenic basins are also located on the Iberian Massif and along the Alpine belts (Fig. 2).

To the north, the Pyrenean–Cantabrian belt consists of the Pyrenees fold-thrust belt and the Cantabrian Mountains. The Pyrenees extend from the Gulf of Lyon in the east to the Gulf of Biscay in the west and were the result of the collision of the Iberian and European plates. The Cantabrian Mountains, uplifted along the North Iberian continental margin, extend from the Basque–Cantabrian basin in the east to the Variscan Cantabrian Zone in the west (Figs. 1 and 2). The belt represents a continental collision with double vergence at upper-mid crustal levels and limited and variable northward subduction of the Iberian crust beneath the European plate. Major structural differences are observed along strike, e.g., amount of convergence, predominance of north vs. south vergences, exhumation of Paleozoic basement or the presence of Mesozoic cover within the thrust system (Pedreira et al., 2007).

Along the southern boundary of Iberia the Betic–Gibraltar–Rif Arc shows an arcuate geometry resulting from a very complex collisional structure involving segmented plate boundaries, whose details are still under debate. Nonetheless, the most recent geodynamic models reconstructing the Neogene evolution of the Central-Western Mediterranean are all based on slab roll-back as the proposed driving mechanism. The main difference being that roll-back starts from different subduction geometries. The majority of the models favor that the basin originated from SE roll-back of a NW-dipping subduction below eastern Iberia (e.g., Faccena et al., 2004; Gueguen et al., 1998; Rosenbaum et al., 2002; Spakman and Wortel, 2004). All these models require a clockwise rotation of the trench of about 180° in order to reproduce the present-day geometry of the Betic orogen. Recently, Vergés and Fernàndez (2012) have presented a new hypothesis in which the Gibraltar Arc system originates from NW roll-back of an initially SE-dipping subduction of the segmented Ligurian-Tethys under the Africa margin.

The Arc comprises an outer zone formed by the Guadalquivir and Gharb (Rharb) foreland basins, the Gulf of Cadiz accretionary complex, the External Betic and Rif thrust systems and the Internal Betic and Rif HP/LT metamorphic complexes (Figs. 1 and 2). The hinterland of this arcuate compressive belt is cut by the extensional system related to the back-arc Alboran basin development (see reviews in Doblas et al., 2007; Vergés and Fernàndez, 2012 and Casciello et al., 2015).

In the *Betic Chain* we distinguish: the Guadalquivir foreland basin and its prolongation into the Gulf of Cadiz mainly composed of Neogene to Quaternary marine sediments; the ENE–WSW trending External Betics, separated into Prebetic and Subbetic domains and consisting of a fold and thrust system piling different SE Iberian passive Mesozoic paleogeographical units towards the foreland (García-Hernández et al., 1980); and the HP/LT metamorphic basement of the Internal Betics that is comprised of a tectonic pile of three different tectonic units each displaying different degrees of Alpine metamorphism.

In the interior of the Iberian plate, convergence led to the formation of the NE–SW Catalan Coastal Ranges and the NW–SE Iberian Chain, mostly preserving the original trends of the previously extended basins (Vergés and Fernàndez, 2006) and to the uplift of some Paleozoic basement blocks. The thin-skin basement uplift zones resulted in the NE–SW to E–W trending Central System and the ENE–WSW oriented Sierra Morena and Toledo Mountains (Casas-Sainz and de Vicente, 2009) (Fig. 2)

3. Geophysical imprints

3.1. Elevation

The elevation data come from ETOPO1 Global Data Base from (http://www.ngdc.noaa.gov/mgg/global). Fig. 3 shows the compiled topography data of the Iberian Peninsula.

Following Casas-Sainz and de Vicente (2009) the average elevation of the Iberian Peninsula is 660 m above sea level, with the highest mean topography located in its northern half (800 m on average) in contrast with the approximately 500 m observed in its southern half (Fig. 3). In the northern half the overall high topography is located in the inner part of the plate (Central System 1064 m; Iberian Chain 895 m or Eastern Duero Basin 843 m), flanked by the Pyrenees–Cantabrian mountains (992 m and 850 m, respectively). In contrast, in its southern half, the high topography is located in the Tajo and High Guadiana Basins (650–700 m) and in the Betic Chain (690 m). In the SW region reliefs are much lower with average values of 386 m in the Toledo Mountains/Guadiana Basin and 140 m in the Guadalquivir Basin (Fig. 3).

According to Vergés and Fernàndez (2006) the most likely cause of the anomalous current topography is the combination of three possible tectonothermal mechanisms acting during different times: a) crustal density variations and possibly mantle depletion during late Paleozoic (Variscan orogeny); b) crustal and mantle lithosphere thickening and folding related to Alpine shortening and c) Neogene and Quaternary upper mantle thinning.

3.2. Geoid

Geoid anomaly data were taken from the EGM2008 spherical harmonic global model (Pavlis et al., 2008) (Fig. 4). The geoid used in the modeling is the residual geoid obtained by filtering up to degree and order 10 to remove wavelengths larger than the study area (see Root et al., 2014 for a detailed analysis of the sensitivity of spherical harmonics degrees).

The most remarkable characteristics of geoid anomalies in the Iberian Peninsula are: i) the geoid relative high (above 3 m) outlining the Iberian Massif and the majority of the uplifted Alpine terrains and ii) the relative lows of the westernmost Betics and the Guadalquivir and Ebro Cenozoic foreland basins where values less than 3 m are observed. The filtered geoid outlines the main topographic features, e.g., the topographic relief of the Pyrenees (above 1000 m) and the anomalous topography of NW, Central and SE Spain (700 m on average) with the exception of the SW region (400 m in average) where the geoid high is up to 8 m (higher than the geoid anomaly recorded at the Pyrenees) (Figs. 3 and 4).

3.3. Gravity

Gravity data on land were taken from a recent compilation carried out by Ayala (2013). The author has integrated all available data onshore and offshore to produce a new gravity map for the entire

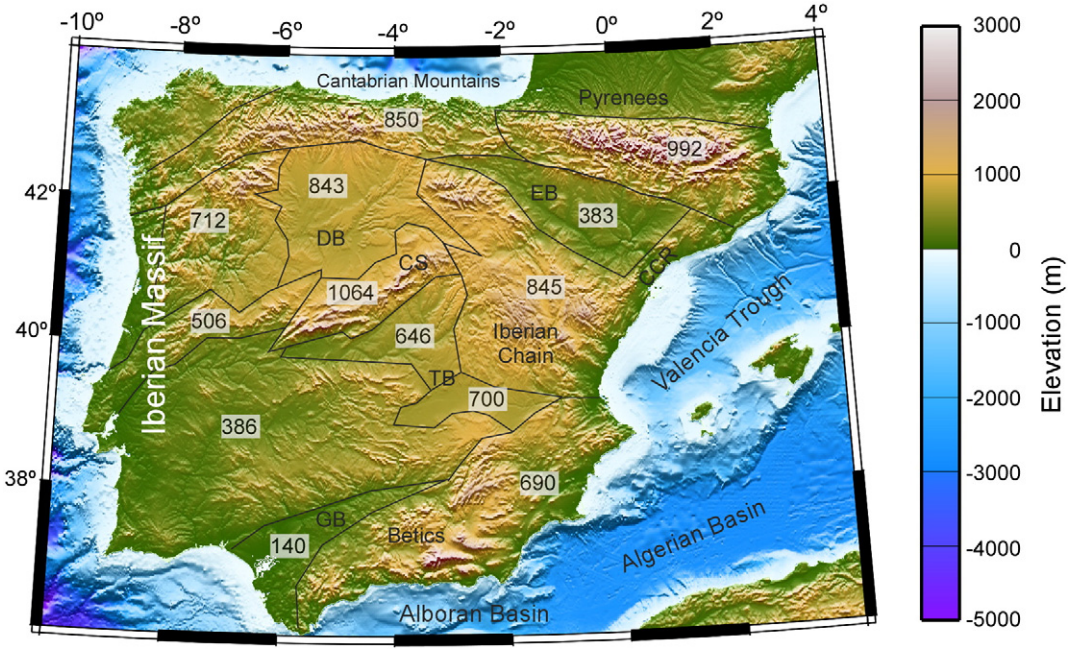

Fig. 3. Elevation map from ETOPO1 Global Data Base Amante and Eakins (2009). Contours every 1000 m. Circled numbers show the average elevation taken from Casas-Sainz and de Vicente (2009).

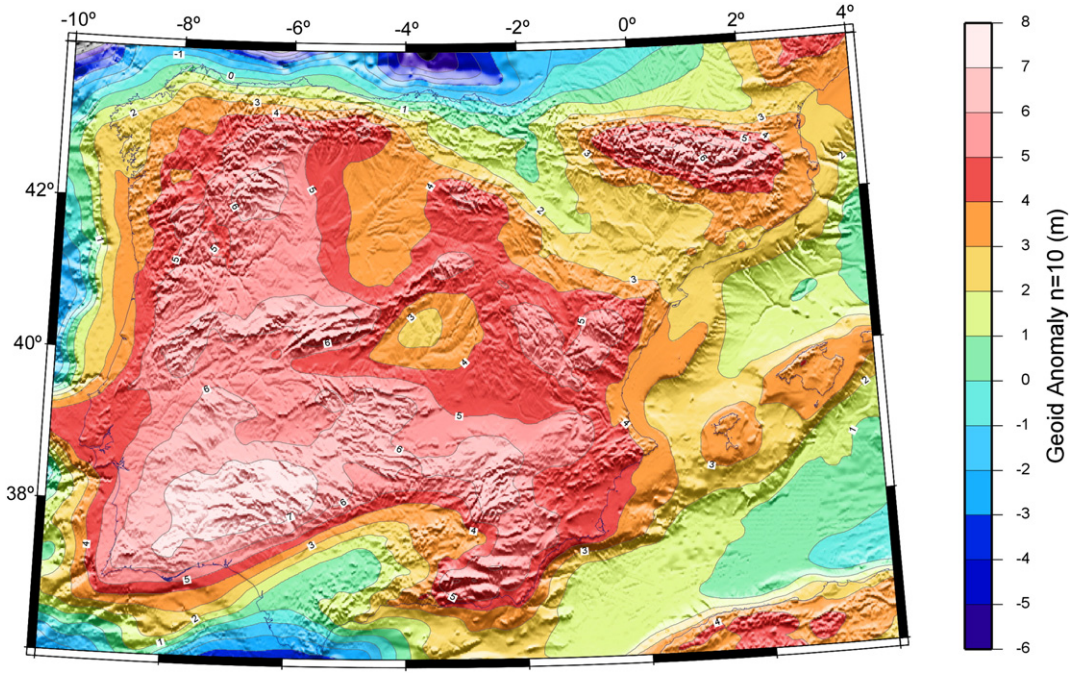

Fig. 4. Geoid anomaly map from EGM2008 spherical harmonic global model (Pavlis et al., 2008). The geoid used in the modeling is the residual geoid obtained by filtering up to degree and order 10 to remove wavelengths larger than the study area. Color key shows geoid anomaly. Contours every 1 m. Shading indicates elevation.

Peninsula and its margins. The most important update being the integration of more than 210,283 data points on land and the use of GRS80 as a geodetic reference system with the associated ETRS89 ellipsoid. The average spatial resolution for the Iberian Peninsula is 1 point for each 2.25 km^2 (see Ayala, 2013 for a more detailed description). The new map has been calculated using a reference density of 2670 kg m^{-3}.

Fig. 5 shows that at a regional scale the Bouguer Anomaly map is characterized by: (i) a regional gravity high located in the SW region of the Iberian Peninsula that delineates the Variscan terranes of the Ossa-Morena and South Portuguese zones with the 0 mGal contour roughly following the boundary between the Central Iberian Zone and the Ossa-Morena zone; and (ii) three regional gravity lows mainly tracing the interplate and intraplate Alpine mountain belts and partially the Tertiary sedimentary basins bounding these belts.

With the exception of its SW region (Ossa-Morena and South Portuguese zones), the Variscan domain does not show a common gravity signature. As seen in Fig. 5 the Cantabrian Zone and West

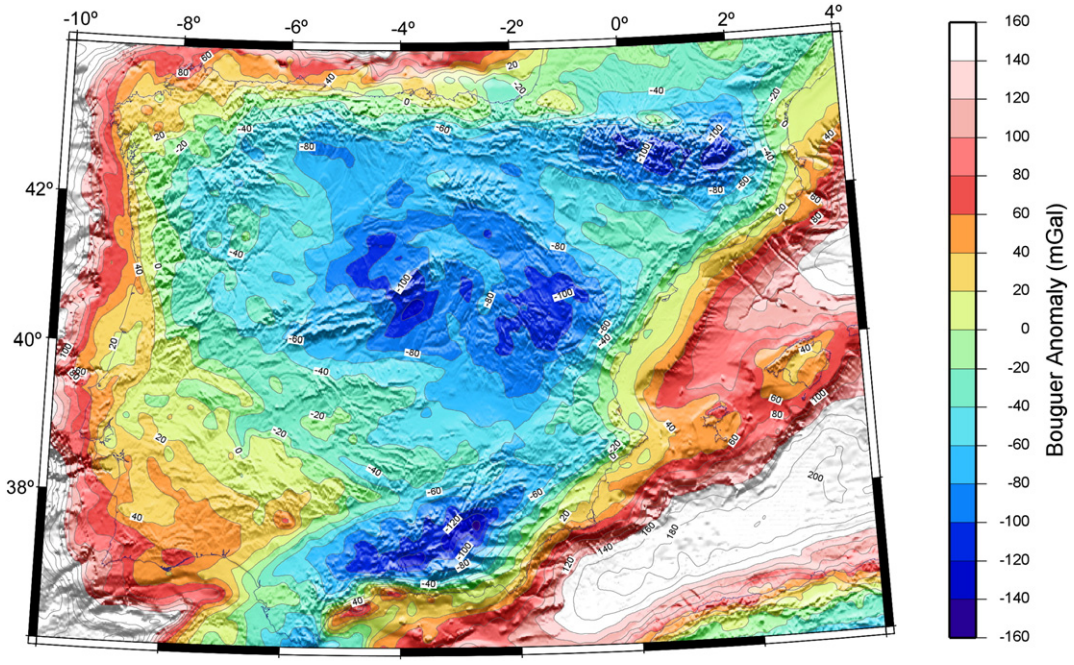

Fig. 5. Bouguer anomaly map from Ayala (2013). The map has been calculated using the geodetic reference system GRS80 and a reference density of 2670 kg m^{-3}. Color key shows Bouguer Anomaly. Contours every 20 mGal. Shading indicates elevation. Access to the data can be found at http://cuarzo.igme.es/sigeco/default.htm.

Asturian–Leonese Zone are characterized by a steep gravity gradient with values ranging from 20 to 40 mGal close to the shoreline to −40 to −50 mGal at the boundary with the Duero Basin, whereas the Central Iberian Zone is characterized by negative gravity anomalies ranging from 0 to −60 mGal, with the exception of its northwestern most corner where gravity highs (0 to 40 mGal) do show the high density terrains of the allochthonous Galicia-Tras-Os-Montes Zone. To the south, the Ossa-Morena and South Portuguese Zones are characterized by positive gravity anomalies that range from 0 to 80 mGal at the southwestern most corner (Cabo de São Vicente), with the 0 mGal contour mainly delineating the Pulo do Lobo orogenic suture zone, which separates the Ossa-Morena and Central Iberia zones, and the 40 mGal contour delineating the oceanic suture zone between the Ossa-Morena and South Portuguese zones.

In contrast, the Alpine domain displays relatively large negative gravity anomalies with three minima related to the Pyrenees, Iberian Chain-Central System and Betics (Fig. 5). The minimum of the Pyrenees is located in the Axial Zone and in the South Pyrenean Thrust System with the lowest values, below −100 mGal, coinciding with an area of crustal thickening and the highest topographic relief of the chain (above 1000 m). On the other hand, the minimum located in the Betics, which displays about the same range of values as in the Pyrenees (−80 to −120 mGal), barely outlines the area of highest reliefs. The minimum with a NE–SW to E–W orientation is mainly located in the central part of the External Betics where seismic data show highly variable crustal thicknesses (see below). The Internal Betics are characterized by a steep NE–SW gravity gradient ranging from −80 mGal at the boundary with the central zone of the External Betics to 20–40 mGal at the shoreline.

The NW–SE oriented gravity low of central Spain ranges from −80 to −120 mGal and comprises the Iberian Chain and the Central System and its associated depocenters of the Duero and Tajo basins (Fig. 5). The Cenozoic Ebro, Duero and Tajo foreland basins show average values from −50 to −60 mGal with the exception of the SE border of the Ebro basin where values of −40 mGal are observed (Fig. 5).

4. Results from previous studies: Crustal and mantle lithospheric structure

During the last decade the Iberian Peninsula has been the target of numerous geological and geophysical surveys to unravel its crustal structure and a few lithospheric profiles and tomography studies that have shed some light on its lithospheric mantle structure and locally on the depth of the base of the lithosphere.

Díaz and Gallart (2009) published a Moho depth map for the Iberian Peninsula and surrounding waters based on the compilation of DSS data. More recently Mancilla and Díaz have analyzed P-to-S conversion phases at the Moho discontinuity from more than 340 broadband stations to estimate the crustal thickness and the Vp/Vs converted ratio. These authors also present a comparison between both data sets and conclude that with the exception of the northern and southern regions (see below), the results have an overall similarity, with most differences in the ±5 km range, inside the error bar estimated for both data sets. Although it is not easy to assign an error bar to those crustal thickness estimations, Waldhauser et al. (1998) consider that the vertical error of the DSS data is on the order of ±3.5 km (optimal case) to ±6 km depending on data quality, modeling and interpolation techniques. Spada et al. (2013) consider that the vertical error for the crustal thickness estimations derived from RF data ranges from ±3 km to ±10 km with the highest errors expected in complex tectonic areas.

Modeling the relief of the crust–mantle boundary, mainly using potential field data, has also been carried out by different authors (Mezcua et al., 1996; Álvarez-García, 2002; Gomez-Ortiz et al., 2011 for the entire peninsula; Vacher and Souriau, 2001 – Pyrenees –; Pedreira et al., 2007 – W Pyrenees–Cantabrian Mountains –, among others).

The Variscan domain is characterized by a relatively flat relief at the base of the crust. Average values range from 30 to 33 km with the exception of the Cantabrian Zone (western segment of the Cantabrian Mountains) where crustal thicknesses reach maximum values of 48–52 km and along the intraplate Central System where the crust is slightly thicker (34 km on average). In SW Iberia, Palomeras et al. (2009) and Ehsan et al. (2015) by means of modeling the normal incidence and wide-angle IBERSEIS and ALCUDIA profiles, respectively, have shown that the crust has a thickness ranging from 31–32 km underneath the western region of the South Portuguese Zone to 34–35 km under the Tajo basin.

On the contrary, the *Alpine domain* shows a more variable relief at the base of the crust and significant discrepancies between DSS and RF results. In the north, a crustal root is evidenced by DSS and RF data (see Fig. 5 of Mancilla and Díaz). Both data sets show Moho depths above 40 km and locally DSS record values above 50 km below the axial zone of the Pyrenees and underneath the western segment of the Cantabrian Mountains. Unlike the Pyrenees, maximum crustal thicknesses recorded along the Cantabrian Mountains do not coincide with the areas of highest relief. A relative thinning to 40 or 46 km, depending on the data set considered, is observed beneath the Basque–Cantabrian Basin. Thinning of the crustal root is observed towards the easternmost Pyrenees (28 km on average) and in the westernmost Cantabrian Mountains at the transition to the Iberian Massif where Moho depths are about 30 to 32 km. On average, RF results depict a crustal root with shallower values for the majority of the belt (in the range of −4 to −8 km) although locally they show a thicker crust.

In the south along the Betics Chain, maximum values of 36–38 km are locally recorded from DSS in the Internal Betics (Sierra Nevada and surroundings), coinciding with high topographic reliefs. Thinning of the crust to less than 25 km is observed towards the External Zones and the easternmost end of the Internal Zones. Differences in the Moho depth on the order of 6 to 8 km are recorded between RF and DSS data all along the central and western segment of the Betics and western onshore termination of the Guadalquivir Basin. In the eastern Betics, these differences can, locally, even exceed 12 km (Fig. 6). Recently, Thurner et al. (2014) from RF analysis of 239 broadband stations found that the Moho depth varies from 25 to 55 km and that there is a strong positive sub-Moho velocity discontinuity at 45–80 km depth beneath the central Betics.

The scarce DSS and the RF data available for the Iberian Chain show that its NW end is characterized by crustal thickness values of 38–40 km whereas its SE end displays values of 30 to 35 km, although locally the Moho is found at about 40 km depth (Zeyen et al., 1985). In its southeastern region up to the transition to the Valencia Trough, thinning of the crust penetrates onshore where DSS record values up to 20 km (Gallart and Díaz, 2013; Zeyen et al., 1985) while RF images display a slightly thicker crust of 24–25 km (Mancilla and Díaz). The Cenozoic Ebro, Duero and Tajo foreland basins show crustal thickness values from 30 to 32 km with some locally thicker values of 36 km in the eastern region of the Duero and Tajo basins and to the NE end of the Ebro basin.

Unlike the base of the crust, the base of the lithosphere is not so well constrained for the whole Iberian Peninsula. Carballo et al. (2015b) found that along the Pyrenees and Ebro Basin the LAB depth oscillates between 130 and 90 km. In the west, underneath the Cantabrian Mountains the lithosphere is thicker with values varying from 125 to 145 km, although locally – under its crustal root – it may reach depths as much as 170 km (Pedreira et al., in press).

In the SW region Fernàndez et al. (2004) using elevation, heat flow, gravity and geoid anomalies showed that beneath the Central Iberian Zone the lithosphere is 110 to 120 km thick, thinning along the Ossa Morena and South Portuguese zones where it reaches minimum values of 95 km. Palomeras et al (2011) along a profile located slightly south, found that the lithosphere is thinner (90 to 110 km) than that obtained by Fernàndez et al. (2004).

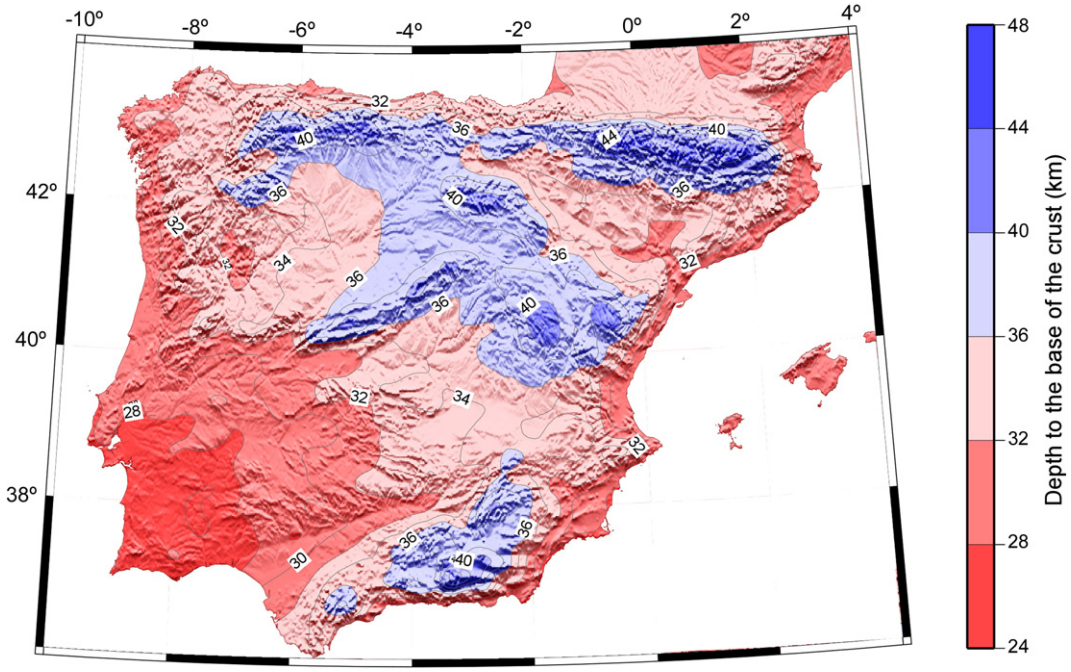

Fig. 6. Resulting crustal thickness obtained from combining elevation and geoid data. Color key shows depth to the Moho. Contours every 4 km. Shading indicates elevation.

Fullea et al. (2010) found a zone of thick lithosphere extending along the western Betics, eastern Rif, Rharb Basin, and Gulf of Cadiz where the lithosphere thickens up to values of 160–170 km. Thinning of the lithosphere towards the easternmost Alboran Basin (from 140 in the Gibraltar strait to less than 45 at the eastern extreme) has been reported by Torne et al. (2000).

5. Modeling approach

The analysis developed in this study is based on a three step approach. In the first step we use the methodology developed by Fullea et al. (2007), which combines elevation, geoid data and thermal analysis. The observed elevation and geoid height are simultaneously fitted assuming local isostasy and considering a four-layer model composed of water, crust, lithosphere mantle and asthenosphere. Therefore, elevation is proportional to $\int \rho(z)dz$, where $\rho(z)$ is the density at a given depth (z). The integral extends from the Earth's surface to the compensation level, which is located below the deepest point of the LAB over the entire modeled region.

Elevation with respect to the sea level is calculated as (Lachenbruch and Morgan, 1990):

$$E = \frac{\rho_a - \rho_L}{\rho_a} \cdot L - L_0 \quad (E > 0)$$
$$E = \frac{\rho_a}{\rho_a - \rho_w} \cdot \left(\frac{\rho_a - \rho_L}{\rho_a} \cdot L - L_0 \right) \quad (E < 0)$$

where E is the elevation, L the total lithospheric thickness, ρ_a = 3200 kg m^{-3} the density of the asthenosphere, ρ_L the average density of the lithosphere and L_0 = 2320 m is the depth of the free (unloaded) asthenosphere level.

Under local isostasy and when lateral density gradients are moderate, the geoid anomaly is proportional to the dipolar moment of the vertical density distribution and then, to $\int z\rho(z)dz$. The geoid anomaly N is calculated by (e.g., Haxby and Turcotte, 1978):

$$N = -\frac{2\pi G}{g} \int z \cdot \rho(z)dz + N_0$$

where G is the universal gravity constant, and g is the gravitational acceleration at the Earth's surface. The integration constant N_0 is calculated by considering a reference column where N and the crustal and lithosphere thicknesses are known.

Note that fixing the crustal and the lithospheric mantle densities; we can calculate the thickness of the crust and the lithospheric mantle from the above equations, which relate elevation and geoid anomaly to lithosphere density distribution. We assume a laterally homogeneous crustal density increasing linearly with depth between a predefined value of 2670 kg m^{-3} at the surface and 2950 kg m^{-3} at the base of the crust, which results in an average crustal density of 2810 kg m^{-3}. Sea-water density is taken to be 1031 kg m^{-3}.

The density of the lithospheric mantle is considered to be temperature dependent (e.g., Lachenbruch and Morgan, 1990) such that $\rho_m(z) = \rho_a\,[1 + \alpha(T_a - T(z))]$, where α is the thermal expansion coefficient (3.5×10^{-5} K^{-1}), and T_a is the temperature at the base of the lithosphere (1330 °C). The depth temperature distribution is calculated by solving the 1D heat transport equation in steady-state:

$$k\frac{d^2T}{dz^2} + A = 0$$

where k is the thermal conductivity and A the volumetric heat production. We consider a thermal conductivity of 2.5 W m^{-1} K^{-1} for the crust and 3.2 W m^{-1} K^{-1} for the lithospheric mantle. The average radiogenic crustal heat production is 1.00 μW m^{-3} (Fernandez et al., 1998; Vilà et al., 2010) and zero for the lithospheric mantle. The above equation is solved with boundary conditions of fixed temperatures at the surface T_s = 0 °C and at the base of the lithosphere (see eqs. 4–32 and 4–33 in Turcotte and Schubert, 2002).

The influence of the thermal parameters on the model results lies in the calculated Moho temperature, which in turn modifies the density of the lithospheric mantle. According to Fullea et al. (2007), the calculated LAB depth decreases almost linearly with increasing thermal expansion coefficient, crustal thermal conductivity and by decreasing the radiogenic heat production. The calculated LAB depth can vary by ±6 km for a wide range of thermal parameters, whereas the crustal thickness is barely affected (~1 km).

Since topographically short wavelengths are partly supported by the rigidity of the lithosphere we have applied a low-pass filter to the elevation data to eliminate wavelengths shorter than 60 km that would result in unrealistic effects in our modeling. The choice of the low-pass filter is based on flexural studies carried out by various authors (e.g., Cloetingh et al., 2002; García-Castellanos et al., 2002; Gaspar-Escribano et al., 2001; Jiménez-Díaz et al., 2012; Ruíz et al., 2006) in which they demonstrate that the rigidity of the Iberian plate seems to be relatively small (elastic thickness in the range of 10 to 30 km).

The reference column consists of a 31.7 km thick crust and a lithospheric thickness of 132.8 km, which, with the densities described above, results in an elevation of 0 m above sea level. This column has been chosen in order to obtain the best fit with the crustal thicknesses obtained from seismic data. Note that the seismic Moho is used to constraint an appropriate reference level for geoid anomalies N_0 (the integration constant of geoid equation) and therefore the reference column.

For a full review of the approach the reader is referred to Fullea et al. (2007). This method has been successfully applied to estimate the crustal and lithospheric mantle geometry of the Gibraltar Arc System (Fullea et al., 2007), the Arabia–Eurasia collision (Jiménez-Munt et al., 2012) and Central Asia (Robert et al., 2015).

In the second step, we separate the measured Bouguer anomaly into its regional and local components. The regional component is calculated from 3D modeling of the crust and mantle lithosphere geometry obtained in step one, using GMSYS-3D commercial software. The 3D model is defined by surface grids with cell-size of 5×5 km. For the crust and lithospheric mantle we have taken the same depth–density distribution as for the 3D model described above. The gravity effect of the model is then calculated in the wavenumber domain with the Parker algorithm (1972) for each of the layers and added together (Popowski et al., 2005). All grids are extended by 50% so they are periodic and eliminate edge effects.

In the third step we invert the residual anomalies resulting from subtraction of the regional gravity field obtained in step two from the observed Bouguer anomaly. For the inversion we keep fixed the base of the crust obtained in step one and allow the inversion algorithm to laterally vary the average crustal density.

6. Results and discussion

In this section we summarize, compare and discuss the results obtained from our modeling with available regional geological, elevation and geophysical data. We also compare the results obtained from assuming crustal versus lithosphere isostasy and discuss the areas that may deviate from local isostasy. Finally we discuss the resulting residual gravity anomalies and their associated lateral average crustal density variations and relate them with the main geological units

6.1. Crust

Fig. 6 shows the base of the crust obtained from our modeling approach. For the majority of the study area the resulting crustal thickness does correlate with the regional topography pattern. Thus, the highest reliefs of the Pyrenees and Betics show crustal thicknesses above 44 km with local values up to 48 km. Crustal thicknesses in the range of 36–40 km are obtained along the uplifted Alpine areas of the Pyrenean–Cantabrian Chain, Betics, and the Iberian Chain as well as the Central System, where topography ranges between 750 and 1500 m. Locally, values above 40 km are registered coinciding with topographic highs. Crustal thicknesses from 32 to 36 km are obtained in the Duero and Tajo basins where the average elevations are 800 m and 640 m, respectively. Ehsan et al. (2015) by use of wide-angle seismic reflection data (ALCUDIA profile) found that the crust under the Tajo Basin is about 34–36 km thick, thinning towards the Central Iberian Zone to 30–31 km. A similar pattern is observed in our crustal model where the crust thins from 36 km at the NE corner of the Tajo Basin to 30 km at the western side of the Central Iberian Zone.

The Ebro basin is characterized by a NW–SE trending crustal thinning towards the uplifted rift shoulders of the Valencia Trough basin with values ranging from 34–36 km at its northwestern most corner to 30 km in the vicinity of the Catalan Coastal Ranges (Fig. 6). To the south, in the Guadalquivir Basin, the crust is slightly thinner than that observed in other Tertiary basins with values from 32 km close to the External Betics to 30 km at the transition to the Sierra Morena Mountains. Notice that the reliefs of the Sierra Morena and Toledo mountains have no crustal expression since they are located within the geoid and gravity highs of SW Iberia (Figs. 4 and 5).

An anomalous NE–SW trending crustal thinning, from 30 to 28 km, is observed in SW Iberia where local geoid and gravity highs (up to 7 m and 60 mGal, respectively) are observed. The resulting crust is slightly thinner (2 to 3 km) than that obtained by Palomeras et al. (2009). These authors, by modeling two 2D wide-angle reflection profiles conclude that in the South Portuguese and Ossa-Morena zones the Moho is located at 31–33 km depth. Pronounced thinning of the crust is also observed close to the shoreline showing the transition to the thin to very thin crust of the Atlantic and Mediterranean margins (González-Fernández et al., 1996, 2001; Pedreira et al., 2007; Torne et al., 1992a,b; Vidal et al., 1998).

In most of the study area our results are in good agreement with seismic data (Figs. 7a and b). For the majority of the region most differences between seismic data and this study are within the range of ± 3 km which falls under the optimal vertical error of the seismic data used in this study (see above). The main differences are registered in the areas where there are significant discrepancies between DSS and RF data. Those regions are: the eastern Cantabrian Mountains and to a lesser extent the axial zone of the Pyrenees, along the Betics, and locally in the SE corner of the Iberian Chain.

Previous studies (e.g., Pedreira et al., 2003, 2007) suggest that the northward underthrusting of the Iberian crust underneath the European crust is a continuous feature that can be traced all along the Pyrenees and Cantabrian Mountains, although the exact style of underthrusting is different from east to west. To the east, in the Central Pyrenees, the Iberian underthrust takes place along a continuous ramp that extends from the South Pyrenean frontal thrust down to the mantle (e.g., Choukroune et al., 1990; Muñoz, 1992). A similar continuous crustal ramp connecting the southern frontal thrust to the mantle is observed along the easternmost part of the Cantabrian Mountains, even though the European lower crust is uplifted to shallower depths, thus dipping steeply to the north (Pedreira et al., 2007). Unlike both regions, in the Central Cantabrian Mountains the Iberian crust sinks into the mantle by a double wedge or double delamination, in which the lower crust of the Cantabrian margin is uplifted and protrudes into the Iberian crust (e.g., Gallastegui, 2000). Consequently along the northern region "two Mohos" can be identified as major discontinuities, the Iberian and the European Moho.

The complexity of the crustal structure observed along the Cantabrian Mountains may explain the significant differences observed between the DSS and RF data and the results obtained in this study (Fig. 7). For the majority of the area DSS show a thicker crust (by 6 to 8 km) when compared to RF results and locally above 10 km. Our results show values closer to the RF results particularly in the Cantabrian Mountains where both modeling approaches suggest a thinner crust (Fig. 7) than that proposed by DSS models. It must be noted however, that according to the above formulation, our methodology does not allow for resolving a 'double Moho' structure. If a "double" Moho exists, our resulting Moho depth will be an averaged value between the two Mohos. As already pointed out by Mancilla and Díaz, the tectonic complexity of the Cantabrian area makes H-κ solutions highly complex, to which should be added the uncertainty of imaging one of the "two Mohos" depending on the orientation and acquisition parameters of the DSS profiles. Furthermore maximum DSS crustal thicknesses (up

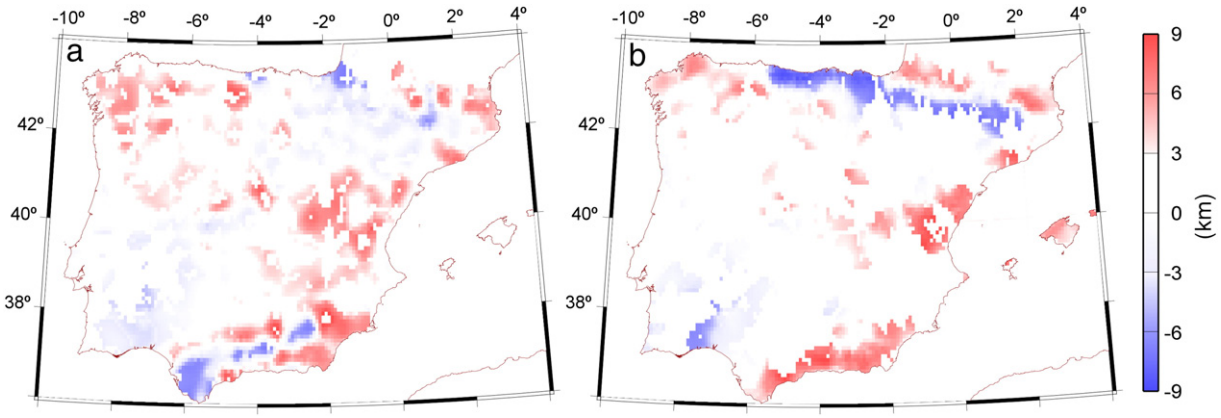

Fig. 7. Differences between the crustal thicknesses obtained from our modelling approach and RF (a) and DSS (b) results. The RF and DSS crustal thicknesses are based on results reported by Mancilla and Díaz (this issue, Fig. 5). Color key shows crustal thickness differences.

to 50 km) are recorded close to the shoreline where topographic relief ranges from 500 to 0 m. This may explain the differences of more than 10 km between our modeling results and DSS data since our assumption is that for its medium-to-long wavelength, the elevation is isostatically compensated. Results from 2D thermal lithospheric modeling performed by Pedreira et al. (in press) and Carballo et al. (2015a-in this volume) show that the European Moho lies at depths of about 30 km, while the Iberian crust may subduct to at least 55 km depth or even deeper (up to 90 km). That fact may explain the differences in the observed Moho depth, since along the same crustal column the Moho can be found at shallower or deeper levels depending on the Moho imaged.

At the southern boundary, along the highest topography of the Internal Betics, our crustal model predicts thicker values than those obtained by DSS and RF data. Local differences around 8 km are observed in both areas (see Fig. 7). To the west, our values show a thinner crust than that obtained by RF data, particularly if we compare them with RF images by Thurner et al. (2014). These authors conclude that the variable depth strong Moho reflectivity observed in the area and an intersecting dipping, positive mantle event may be indicative of ongoing lithospheric delamination, with the detachment surface being the continental Moho.

The results obtained for the Iberian Chain show an average crustal thickness of 36 km with three local values above 40 km located at its NE corner and at the SE region (Fig. 6), which is within the range of agreement with seismic data (Díaz and Gallart, 2009; Gallart and Díaz, 2013 and Mancilla and Díaz. The misfit observed at the SE most end of the chain (Fig. 7) is likely to be related to the opening of the Valencia Trough basin and the consequent crustal thinning entering onshore (Gallart and Díaz, 2013; and Zeyen et al., 1985).

6.2. Lithospheric mantle

Fig. 8 shows the resulting lithospheric thickness. The thickest lithosphere – above 150 km – is found underneath the Pyrenees. Thick lithosphere – from 140 to 150 km – is obtained along the Cantabrian Mountains, the Iberian Chain, the western Central System, and in the

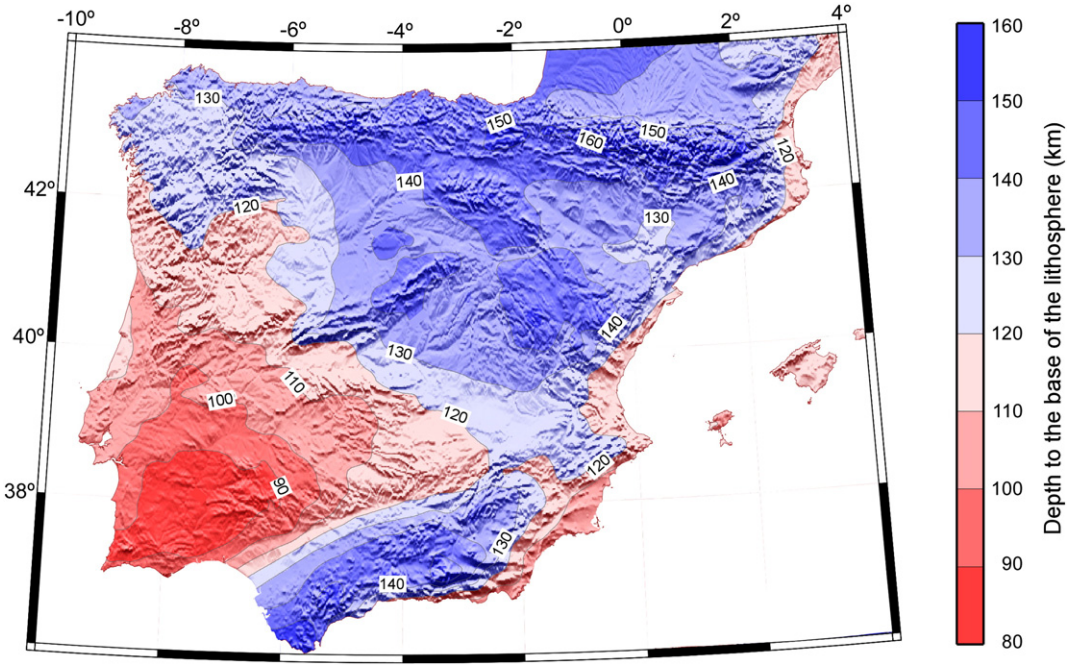

Fig. 8. Resulting lithospheric thickness obtained from combining elevation and geoid data. Color key shows depth to the LAB, Lithosphere–Asthenosphere Boundary. Contours every 5 km. Shading indicates elevation.

Betics. Underneath the eastern Central System, the Ebro basin, the Duero and Tajo basins and in the northern corner of the Iberian Massif lithospheric thicknesses range from 120 to 140 km. Towards the SW, the lithosphere thins steadily to minimum values of 90 km, thus indicating that the Variscan lithosphere (Iberian Massif) is overall thinner than the Alpine lithosphere of the Iberian Peninsula (Fig. 8).

For the Pyrenean–Cantabrian belt our results show that its overall trend is in agreement with those obtained by Pedreira et al. (in press); Carballo et al. (2015b) and Carballo et al. (2015a-in this volume). Pedreira and co-authors conclude that the thickness of the lithosphere onshore varies from 125 to 145 km south of the Cantabrian Mountains, although locally it may reach values up to 170 km underneath the crustal root. Carballo et al. (2015a-in this volume) find that beneath the Duero Basin, Central System and the Tajo Basin the lithosphere thickness is very close to our calculated values. Along the Pyrenees and Ebro Basin our results agree with those obtained by Carballo et al. (2015b). These authors by modeling a 2D transect report that the LAB depth varies from about 140 km beneath the Pyrenees to 100 km at the shore line. We also obtain a similar NW–SE lithosphere thinning towards the extended lithosphere of the Valencia Trough.

A remarkable result is the mass deficit at deep lithospheric mantle levels necessary to fit the observed anomalous geoid height and elevation over the Ossa-Morena and South Portuguese zones. Such mass deficit could be interpreted as a lithospheric thinning that agrees with the results reported by Fernàndez et al. (2004); Fullea et al. (2007) and Palomeras et al. (2011). Fernàndez et al. (2004) show that the lithosphere beneath the south Iberian Massif is about 95 km thick. They conclude that the observed geoid and gravity anomalies may be interpreted either by lithospheric thinning or as an anomalous density reduction of ~25 kg m^{-3} affecting the lower lithospheric levels. The first hypothesis is consistent with a possible thermal anomaly related to recent geodynamics affecting the nearby Gibraltar Arc system, the second with mantle depletion occurring during the late Paleozoic continental collision between Laurasia and Gondwana (Variscan orogeny). On the southern edge, the Betic region is characterized by lithospheric thickening with values above 130 km.

Our results also show that surface heat-flow values are in the range of 58 to 70 mWm^2. The lowest values (less than 60 mWm^2) are recorded in the Ebro and Basque–Cantabrian basins to the North, and the western Betics and the Guadalquivir basin, to the South. The highest values (above 65 mWm^2) are observed in the Ossa Morena and South Portuguese Zones. For the majority of the study area values range from 60 to 65 mWm^2 in fairly good agreement with the average measured heat flow (Fernandez et al., 1998).

Fig. 9 compares the base of the crust and LAB considering crustal isostasy (i.e. topography is fully compensated at the base of the crust), lithosphere isostasy (i.e. pure-shear lithospheric deformation) and joint modeling of geoid and elevation combined with thermal analysis used in this study. When comparing the calculated base of the crust with that obtained assuming crustal isostasy, we infer that for the Alpine domain the main features and trends are in good agreement. The main difference being that overall the crust obtained in our study is slightly thinner (1 km on average) with the exception of the SW Iberia regions where values up to 6 km are achieved. Major differences in the crustal thickness are observed under the assumption of lithosphere isostasy. A thicker Moho (up to 9 km) is found underneath the Pyrenees

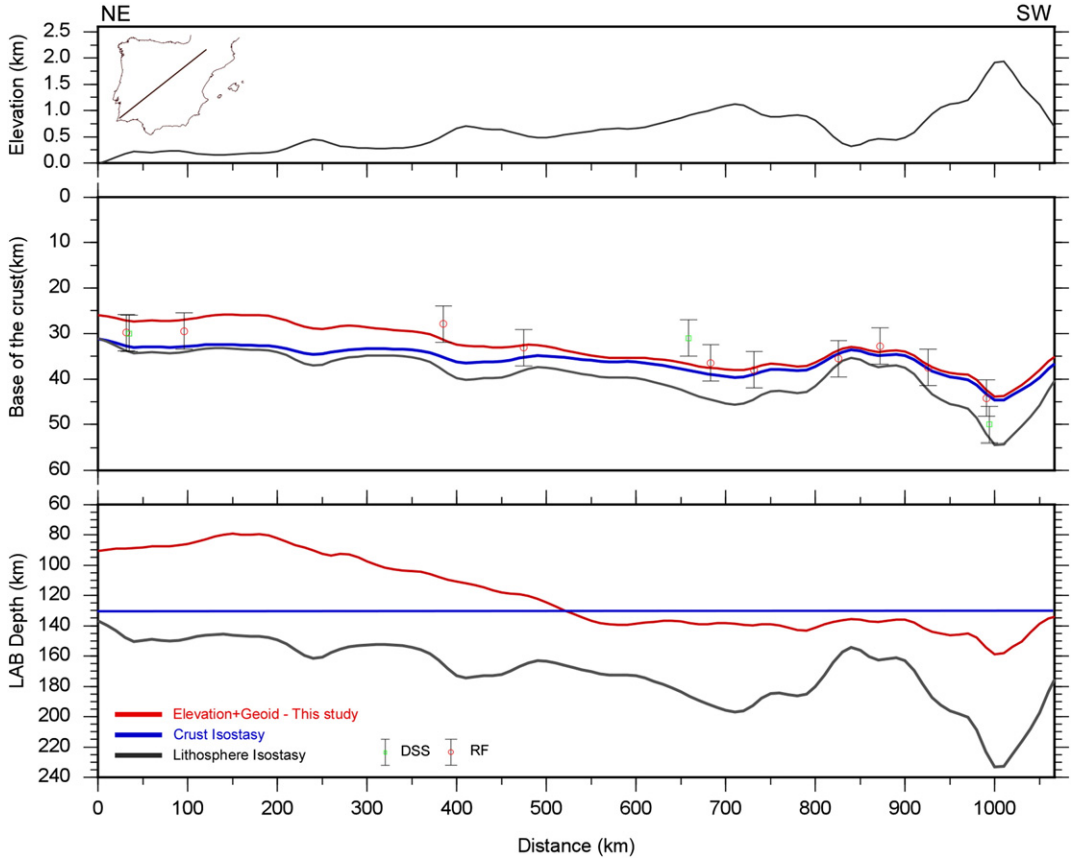

Fig. 9. Comparison between different methods of calculating the Moho and LAB depths, along the NE–SW profile located in the upper left inset. Each color represents the result from: red for combining geoid and elevation; blue for crustal isostasy (Airy) and black for lithosphere isostasy. The observed differences arise from the fact that crustal isostasy assumes that the base of the lithosphere is flat, whereas lithosphere isostasy assumes pure-shear lithospheric deformation.

and in SW Iberia. Differences between the LAB obtained by joint modeling of geoid and elevation and that obtained assuming lithosphere isostasy (pure-shear deformation) are in the range of 40 to 50 km.

The calculated geoid and regional Bouguer gravity field can differ significantly from that calculated under the assumption of crustal (Airy) isostasy or from lithosphere isostasy. The differences arise from the fact that crustal (Airy) isostasy assumes that the base of the lithosphere is flat, whereas lithosphere isostasy assumes pure-shear lithospheric deformation. Indeed, these two isostasy approaches only consider elevation as a constraint (see Jiménez-Munt et al., 2012 for a thorough discussion).

6.3. Residual gravity field

The residual gravity anomalies and the lateral average crustal density variations obtained from 3D inversion of these anomalies are shown in Fig. 10. The calculated residual gravity anomaly map shows wide regions with residuals between −10 to 10 mGal (Fig. 10). Accordingly, in this section we discuss those anomalies that are above or below the mentioned interval. We distinguish 7 main anomalies located at: the Southern Iberian Massif (A and B); the Northern Iberian Massif (C); the foreland basins of the Central System (D); the Western Ebro Basin and NE Iberian Chain (E); the Pyrenees (F1 and F2); and the Betics (G, H and H′).

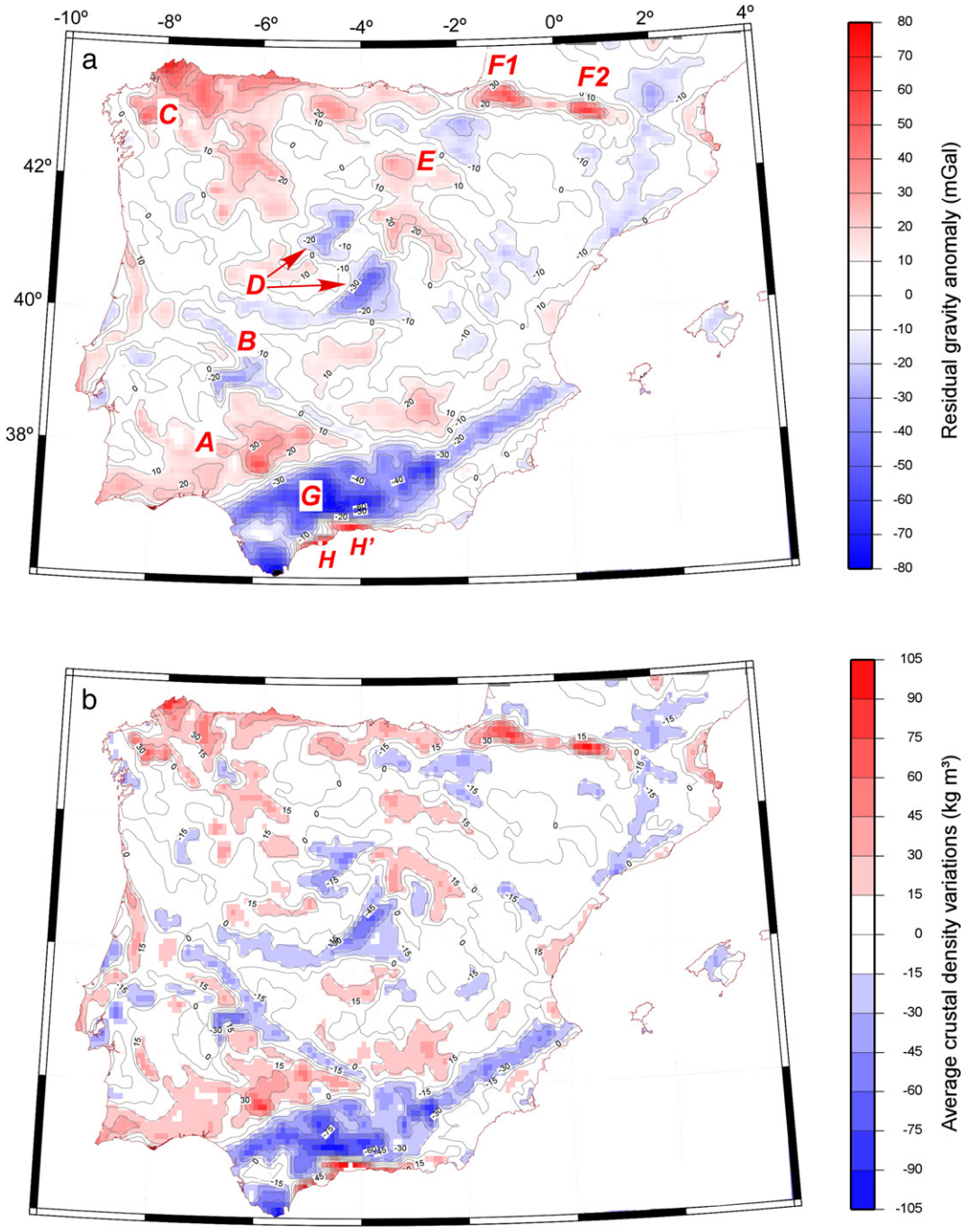

Fig. 10. a) Residual Bouguer anomaly resulting from subtracting the measured Bouguer anomaly from the 3D gravity effect of the lithospheric structure obtained from combining elevation and geoid data. We distinguish 7 main residual anomalies located at: the southern Iberian Massif (A and B); the northern Iberian Massif (C); the foreland basins of the Central System (D); the western Ebro Basin and NW Iberian Chain (E); the Pyrenees (F1 and F2); and the Betics (G, H and H′). Contours every 10 mGal. b) Lateral average crustal density variations deduced from 3D inversion of the residual gravity anomalies shown in Fig. 10a. Contours every 15 kg m^{-3}.

6.3.1. The Southern Iberian Massif (A and B)

The positive residual anomaly located in the southern region of the Iberian Massif (A in Figs. 10a) likely indicates that, either the average density of the crust is denser than the adopted crustal density column or that the Moho is located at shallower depths. Our preferred interpretation is the former since the calculated Moho depths are slightly shallower than those obtained by Palomeras et al. (2009). 3D inversion of the residual gravity anomalies (see Fig. 10b) also shows an increase of the average crustal density in the range of 15 to 30 kg m^{-3}.

Furthermore, under the South Portuguese Zone and southern boundary of the Ossa-Morena Zone, Palomeras et al. (2009, 2011) report the presence of high-velocity/high-density lenses at mid-crustal levels (6.8–7.0 km s^{-1}). The authors conclude that the densities of these high velocity lenses – one of them also depicted along the IBERSEIS normal incidence profile as a highly reflective body (IRB) (Carbonell et al., 2004) – range from 2950 to 2990 kg m^{-3}. The presence of this high density middle crust results in an average crustal density of 2840 ± 10 kg m^{-3}, which is in agreement with the results obtained in our study. As seen in Fig. 10b the residual gravity high requires an increase of the average crustal density of 15 to 30 kg m^{-3}.

The very local residual gravity high of up to 40 mGal located in the NE corner of the South Portuguese Zone falls within the high-density Beja-Acebuches amphibolite complex and corresponds to an increase of the average crustal density above 75 kg m^{-3}. Close to the boundary between the Central Iberian and Ossa-Morena Zones (B in Fig. 10) there is a NW–SE oriented narrow and elongated negative anomaly coinciding with the outcrop of granitic rocks. The low E–W trending anomaly roughly delineates the Tertiary and Quaternary sediment infill of the Badajoz and Guadiana Basins and requires a decrease in the average crustal density of −30 to −45 kg m^{-3}.

6.3.2. The Northern Iberian Massif (C)

To the north and from west to east the Galicia-Tras-Os-Montes Zone (GTOMZ), and the Cantabrian and Asturian–Leonese Zones are characterized by a regional positive residual of 10 to 20 mGal that locally may reach values above 30 mGal. The regional positive residual that extends further to the SE (C in Fig. 10a) indicates that the crust is slightly denser (20 kg m^{-3} on average) than that assumed in our model (Fig. 10b). The local residual highs of the GTOMZ (NW and SE corners) are related to the high density allochthonous complexes, mainly composed of ultramafic rocks, eclogites and high-pressure granulites and ophiolites (Ábalos et al., 2003).

6.3.3. The foreland basins of the Central System (D)

Local negative residuals are observed along the Duero and Tajo depocenters of the Central System. These depocenters are characterized by thicknesses of 2500 and 3000 m and densities in the range of 2300–2400 kg m^{-3} (de Vicente et al., 2007). The relative low density of the sedimentary infill when compared to our density profile at depths between 2 to 3 km (2690 kg m^{-3} on average) helps explain the negative residual associated with both areas. The 3D inversion of the residual gravity anomalies shows that the average crustal density diminishes by as much as −50 kg m^{-3} where maximum sedimentary thicknesses are recorded (Fig. 10b).

6.3.4. The Western Ebro Basin and the NW Iberia Chain (E)

A negative residual anomaly, with similar characteristics to the ones observed in the Duero and Tajo basins, is observed at the western termination of the Ebro basin as well as in the eastern border of the Basque–Cantabrian thrust sheet (Fig. 10a). The residual gravity low located at the western termination of the Ebro basin is likely related to the presence of thick sedimentary sequences including large amounts of Oligocene–Miocene evaporites (e.g., Riba and Jurado, 1992). This negative anomaly continues beneath the connecting zone between the external Western Pyrenees and the Basque–Cantabrian Thrust Unit. The anomaly could correspond to the northern continuation of the Oligocene evaporites in the footwall of the Pyrenean Thrust System and/or be due to extensive Upper Triassic diapirs along the hanging wall of the Pamplona Fault (e.g., Larrasoaña et al., 2003; Vergés, 2003). The increase of average crustal density to the NW region of the Iberian Chain is likely related to the outcrop of Paleozoic basement rocks.

6.3.5. The Pyrenees (F1 and F2)

Two local residual highs are observed in the western and center Aquitaine basin along the Northern Pyrenees (F1 and F2 in Fig. 10a). The first one (F1), showing maxima of 40 mGal, corresponds to the Labourd Massif anomaly (Mauléon basin or South Lacq basin as well as its westwards continuation within the north-directed Pyrenean fold belt; e.g., Biteau et al., 2006). The second one (F2), with maxima of 80 mGal, fits with the Saint-Gaudens anomaly (Comminges flysch basin ahead of the North Pyrenean thrust front). Note that these positive residual anomalies are located in deep sedimentary basins with up to 7000 m of infill (Biteau et al., 2006). 3D inversion of the residual gravity anomalies shows that the average density of the crust has to be increased to as much as 70 kg m^{-3} in the Labourd Massif area and above 90 kg m^{-3} in the Comminges flysch basin.

Torne et al. (1989) reported a positive gravity anomaly around Saint Gaudens on the French side of the ECORS-Pyrenees deep seismic profile (F2 in Fig. 10a). Vacher and Souriau (2001) pointed out the extent of these positive anomalies in the Bouguer anomaly map (Labourd Massif and Saint-Gaudens in the east) (see Fig. 5) as was already defined in tomography studies carried out by Souriau and Granet (1995).

The close spatial relationships between outcropping lherzolites and granulites along the North Pyrenean Fault Zone (e.g., Vielzeuf and Kornprobst, 1984) and the obtained residual positive anomalies led to proposing the presence of high density bodies varying in density, extent and depth depending on their position. Thus, Torne et al. (1989) interpreted the anomaly as either a relatively shallow (from 1 to 12 km) narrow high-density body (2930 kg m^{-3}) corresponding to a slice of lower crust, based on seismic fabrics, or to various intracrustal mantle slices in agreement with the presence of outcropping lherzolites. Vacher and Souriau (2001), from 3D gravity modeling and considering previous results from Souriau and Granet (1995), concluded that the Labourd Massif anomaly may be explained by the presence of a high-density body (2930 to 2950 kg m^{-3}) that extends to 12 km depth, becoming laterally wider below 7 km and then narrowing again until a depth of 12 km. The Saint-Gaudens anomaly is attributed to the presence of a high density block about 60 km long, 25 km wide and extending from 7 to 15 km (Vacher and Souriau, 2001). Recently, Macquet et al. (2014) using a high-resolution 3D S-wave velocity model for the Pyrenees and adjacent areas concluded that the positive gravity anomaly located at the Labourd–Mauléon–Arzacq region can also be correlated with a high S-wave velocity anomaly at 20–30 km depth.

The overlap of these positive anomalies caused by high-density bodies at depth with thick sedimentary basins could indicate a linked genetic origin as suggested in Macquet et al. (2014) and attributed to the Aptian–Albian rifting event. The importance of such extensional events related to large exposures of mantle rocks flooring the sedimentary basins in the Central and Western Pyrenees has been shown in recent works (e.g., Jammes et al., 2009; Lagabrielle et al., 2010).

6.3.6. The Betics (G, H and H′)

Lastly, the most remarkable result that we present is the wide NE–SW trending residual gravity low that lies below the Central and West External Betics and the Guadalquivir basin (Fig. 10a). The residual gravity low largely correlates with the surface extent of the Subbetic unit, belonging to the External Betics, as imaged in the geological map. In detail, however, the negative anomaly extends well beneath the SSE sector of the Guadalquivir basin in addition to having limited extent below few areas of the Internal Betics. Inversion of the residual gravity low shows that the crust is less dense in the range of −30 to

−40 kg m^{-3} than the average crustal density assumed in this study, although locally may decrease to as much as 80 kg m^{-3} (Fig. 10b).

The regional anomaly is interpreted here as having resulted from the combined effect of shallow and deep sources. At upper crustal levels, thick accumulation of both Triassic evaporites and shales and late Jurassic–Early Cretaceous basinal marine deposits (e.g., García-Hernández et al., 1980; Vera, 2004) partly explain the residual gravity low. The Upper Triassic evaporites constitute the detachment level along the basal thrust of the Subbetic unit and thus thick accumulations of them may occur in addition to diapir structures of different sizes (e.g., Crespo-Blanc, 2007; Pedrera et al., 2014; Vergés and Fernàndez, 2012; Wildi, 1983). To this we have to add the thicker crust recorded by seismic experiments (see above) resulting in a density deficit with respect to the chosen crustal column and also the presence at mantle depths of a detached slab that may result in the whole area departing from our assumption of local isostasy.

The extent of the negative anomaly beneath the Guadalquivir basin in the Western Betics could be related to the emplacement of a massive "chaotic unit" (Fernandez et al., 1998) located at the frontal wedge of the External Betics. According to these authors this unit mainly consists of undercompacted shales and clays with intervals of Triassic evaporites and its thickness may be as much as 2600 m (Fernandez et al., 1998). An approximate calculation of the effect of the sedimentary infill of the Guadalquivir Basin considering a constant density of 2400 kg m^{-3} gives values of as much as −40 mGal.

The potential continuation of the negative anomaly beneath the Internal units in a few local areas may correspond to a change in the tectonic structure of the External–Internal boundary thrust. In the Central Betics, the Internal units form a tectonic wedge beneath the External units whereas towards the Western Betics the Internal units are thrusted over the External units (e.g., Platt et al., 2003). In this context, the extent of the negative anomaly below the Internal units can be the result of low density sedimentary units (Subbetic units) in the footwall of the Internal units' basal thrust.

Along the southern outcropping boundary of the Internal units there are two strong residual positive anomalies (Fig. 10a, H and H′) that have their continuation in the Beni-Bousera region in the Rif in Morocco (e.g. Torne et al., 1992a). The positive anomaly near Marbella has been modeled as a peridotite body that is ~70 km wide along an ENE–WSW tectonic grain trend, 8 km thick and 40 km long in a NNW–SSE direction (Torne et al., 1992a). Residual anomaly H′ may correspond as well to a peridotite unit that is slightly displaced towards the north but displaying a similar tectonic trend. Inversion of both gravity highs shows an increase of the average crustal density in the range of 70 to 80 kg m^{-3} (Fig. 10b).

7. Concluding remarks

In this study we present a model of the lithospheric structure of the Iberian Peninsula obtained from joint modeling of elevation and geoid anomaly data combined with steady state thermal analysis. The main assumptions are that elevation is isostatically compensated at the base of the lithosphere and that the thermal regime is in steady state. We also assume a linear density increase with depth for the crust and a temperature dependent density for the lithospheric mantle. 3D forward gravity modeling has allowed verifying the feasibility of the proposed lithospheric structure while 3D inversion of the residual gravity anomalies has allowed correlating lateral average density variations in terms of crustal structures and geological domains.

Our model agrees fairly well in its overall pattern to previous seismic experiments and 2D modeling results. For the majority of the study area the resulting crustal thickness does correlate with the regional topographic pattern and is in good agreement (±3 km) with available seismic data. While the crust in the Variscan domain is characterized by a relatively flat Moho and a thin lithosphere, the Alpine domain in contrast shows a more variable Moho relief and a thicker lithosphere. The thickest lithosphere (above 150 km) is found along the Pyrenees–Cantabrian belt while the thinnest (90 km) is found in the SW Iberian Peninsula.

A remarkable result is the conspicuous lithospheric thinning affecting the SW-Iberia region that we interpret to be related to recent extensional geodynamic events affecting the Betic–Gibraltar–Rif orogenic system. However, we cannot rule out chemical depletion by partial melt extraction from the deeper levels of the lithospheric mantle occurring during the late Paleozoic continental collision between Laurasia and Gondwana (Variscan orogeny) (Fernàndez et al., 2004).

The highest reliefs of the Pyrenees and Betics show crustal thickness above 44 km with local values above 48 km. Crustal thicknesses in the range of 36–40 km are obtained along the uplifted Alpine regions, whereas along the Cenozoic foreland basins the crust is slightly thinner, from 32 to 36 km.

Major discrepancies of the obtained crustal thicknesses with existing data are observed in the North and South of Iberia where there are complex 3D tectonic settings and where DSS and RF data also show significant differences. To the North, in the Cantabrian Mountains discrepancies may locally rise up to 8 km and are likely related to the presence of a "double Moho" which is difficult to image even by DSS models and RF analysis. Along the Pyrenean–Cantabrian belt our results are better suited to those obtained by RF analysis. To the south, in the Gibraltar Arc region the most plausible explanation is delamination such that the area departs from local isostasy due to the presence of a recently detached/torn lithospheric slab at deep levels.

Along the Betic Chain and Guadalquivir Basin, the negative anomaly results from the combined effect of shallow and deep sources. At crustal levels, the presence of low density deposits combined with the thicker crust imaged by seismic experiments may result in a mass deficit not covered by our density crustal column. At depth, the presence of a detached/torn slab may result in a strong departure from local isostasy.

Positive anomalies are related to relatively high-density outcropping ultramafic rocks (North Iberian Massif), Paleozoic metamorphic rocks (NW-Iberian Chain), or mid-crustal high-velocity/high-density bodies (South Iberian Massif, Pyrenees and Internal Betics). Negative anomalies are related either to the low density sedimentary infill of the Duero and Tajo foreland basins (Central System), Badajoz and Guadiana basins (Ossa-Morena Zone), and the east Ebro Basin; or to granitic outcrops (contact between the Central Iberian and Ossa-Morena zones).

3D inversion of residual anomalies shows that for the majority of the study area the average density of the crust is in the range of 2810 kg m^{-3} ± 10 kg m^{-3}. The denser crust is found in the NW and SW regions of the Iberian Massif (+30 kg m^{-3} on average) and locally in the Pyrenees (above +70 kg m^{-3}), NW of the Iberian Chain (+15 kg m^{-3} on average) and in southern Internal Betics (above +70 kg m^{-3}). The least dense crust is found in the central and western Betic Chain (−30 kg m^{-3} on average) and in sedimentary basin depocenters.

Acknowledgments

This research has been funded by the WE-ME project (PIE-CSIC-201330E111) and TECLA project (Spanish National Research and Innovation Plan, CGL2011-26670). We deeply acknowledge the comments and suggestions made by J. Ebbing and an anonymous reviewer that helped to improve the first manuscript. Figs. 3–10 were made using GMT (Wessel and Smith, 1998).

References

Ábalos, B., Puelles, P., Gil Ibarguchi, J.I., 2003. Structural assemblage of high-pressure mantle and crustal rocks in a subduction channel (Cabo Ortegal, NW Spain). Tectonics 22 (2), 1006. http://dx.doi.org/10.1029/2002TC001045.

Álvarez-García, J., 2002. Análisis gravimétrico e isostático en el Macizo Ibérico. http://eprints.ucm.es/5898/.

Amante, C., Eakins, B.W., 2009. ETOPO1 1 Arc-Minute Global Relief Model: Procedures, Data Sources and Analysis. NOAA. Technical Memorandum NESDIS NGDC-24. National Geophysical Data Center, NOAA. http://dx.doi.org/10.7289/V5C8276M.

Ayala, C., 2013. A new compilation of gravity data over the Iberian Peninsula and surrounding areas. Internal Report TopoIberia project (Consolider-Ingenio). IGME (20 pp., 3 figures. http://www.ictja.csic.es/images/Documents/FinalReportGravityTopoIB.pdf).

Bezada, M.J., Humphreys, E.D., Toomey, D.R., Harnafi, M., Dávila, J.M., Gallart, J., 2013. Evidence for slab rollback in the westernmost Mediterranean from improved upper mantle imaging. Earth Planet. Sci. Lett. 368, 51–60. http://dx.doi.org/10.1016/j.epsl.2013.02.024.

Biteau, J.J., Le Marrec, A., Le Vot, M., Masset, J.M., 2006. The Aquitaine Basin. Pet. Geosci. 12 (3), 247–273. http://dx.doi.org/10.1144/1354-079305-674.

Bonnin, M., Nolet, G., Villaseñor, A., Gallart, J., Thomas, Ch., 2014. Multiple-frequency tomography of the upper mantle beneath the African/Iberian collision zone. Geophys. J. Int. 198, 1458–1473. http://dx.doi.org/10.1093/gji/ggu214.

Carballo, A., Fernàndez, M., Jiménez-Munt, I., Torne, M., Vergés, J., Melchiorre, M., Pedreira, D., Afonso, J.C., García-Castellanos, D., Díaz, J., Villaseñor, A., Pulgar, J.A., Quintana, L., 2015a. From the North-Iberian Margin to the Alboran Basin: a lithosphere geo-transect crossing the Iberian Plate (submitted), Tectonophysics (in this volume).

Carballo, A., Fernàndez, M., Torne, M., Jiménez-Munt, I., Villaseñor, A., 2015b. Thermal and petrophysical characterization of the lithospheric mantle along the northeastern Iberia geo-transect. Gondwana Res. http://dx.doi.org/10.1016/j.gr.2013.12.012.

Carbonell, R., Pérez Estaún, A., Simancas, J.F., Juhlin, Ch., Pous, J., González Loreiro, F., Muñoz, G., Heise, W., Ayarza, P., 2004. Geophysical evidence of a mantle derived intrusion in SW Iberia. Geophys. Res. Lett. 31 (L11601), 1–4. http://dx.doi.org/10.1029/2004GL019684.

Casas-Sainz, A.M., de Vicente, G., 2009. On the tectonic origin of the Iberian topography. Tectonophysics. http://dx.doi.org/10.106/j.tecto.2009.01.030.

Casciello, E., Fernàndez, M., Vergés, J., Cesarano, M., Torne, M., 2015. The Alboran Domain in the Western Mediterranean evolution: the birth of a concept. In: Seranne, M., et al. (Eds.), Lithosphere Dynamics and Sedimentary Basins: the Circum-Mediterranean Basins and Analogues. Bull. Soc. Géol. Fr. 186.

Chevrot, S., Villasenor, A., Sylvander, M., Benahmed, S., Beucler, E., Cougoulat, G., Delmas, P., Blanquat, M.D., Díaz, J., Gallart, J., Grimaud, F., Lagabrielle, Y., Manatschal, G., Mocquet, A., Pauchet, H., Paul, A., Pequegnta, C., Quillard, O., Roussel, S., Ruiz, M., Wolyniec, D., 2014. High-resolution imaging of the Pyrenees and Massif Central from the data of the PYROPE and IBERARRAY portable array deployments. J. Geophys. Res. Solid Earth 119 (8), 6399–6420. http://dx.doi.org/10.1002/2014JB010953.

Choukroune, P., Roure, F., Pinet, B., ECORS Pyrenees Team, 1990. Main results of the ECORS Pyrenees profile. Tectonophysics 173 (1–4), 411–418 (20).

Cloetingh, S., Burov, E., Beekman, F., Andeweg, B., Andriessen, P.A.M., Garcia-Castellanos, D., de Vicente, G., Vegas, R., 2002. Lithospheric folding in Iberia. Tectonics 21 (5), 1041. http://dx.doi.org/10.1029/2001TC901031.

Crespo-Blanc, A., 2007. Superimposed folding and oblique structures in the paleomargin-derived units of the Central Betics (SW Spain). J. Geol. Soc. 164, 621–636. http://dx.doi.org/10.1144/0016-7692006-084.

De Vicente, G., Vegas, R., Muñoz Martín, A., Silva, P.G., Andriessen, P., Cloetingh, S., González Casado, J.M., Van Wees, J.D., Álvarez, J., Carbó, A., Olaiz, A., 2007. Cenozoic thick-skinned deformation and topography evolution of the Spanish Central System. Glob. Planet. Chang. 58, 335–381. http://dx.doi.org/10.1016/j.gloplacha.2006.11.042.

Dercourt, J., Zonenschain, L.P., Ricou, L.E., Kazmin, V.G., Le Pichon, X., Knipper, A.L., Grandjacquet, C., Sbortshikov, I.M., Geysssant, J., Lepvier, C., Pecheresky, D.H., Boulin, J., Sibouet, J.C., Savostin, L.A., Sorokhtin, O., Westphal, M., Bazhenow, M.L., Lauer, J.P., Biju-Duval, 1986. Geological evolution of the Tethys belt from the Atlantic to the Parmis since the Lias. Tectonophysics 123, 241–315.

Díaz, J., Gallart, J., 2009. Crustal structure beneath the Iberian Peninsula and surrounding waters: a new compilation of deep seismic sounding results. Phys. Earth Planet. Inter. 173, 181–190. http://dx.doi.org/10.1016/j.pepi.2008.11.008.

Díaz, J., Gil, A., Gallart, J., 2013. Uppermost mantle seismic velocity and anisotropy in the Euro-Mediterranean region from Pn and Sn tomography. Geophys. J. Int. 192, 310–325. http://dx.doi.org/10.1093/gji/ggs016.

Doblas, M., López-Ruiz, J., Cebriá, J.M., 2007. Cenozoic evolution of the Alboran Domain: a review of the tectonomagmatic models. In: Beccaluva, L., Bianchini, G., Wilson, M. (Eds.), Cenozoic Volcanism in the Mediterranean Area. Geological Society of America Special Paper 418(15), pp. 303–320.

Ehsan, S.A., Carbonell, R., Ayarza, P., Martí, D., Martínez Poyatos, D., Simancas, J.F., Azor, A., Ayala, C., Torne, M., Pérez-Estaún, A., 2015. Lithospheric velocity model across the Southern Central Iberian Zone (Variscan Iberian Massif): the ALCUDIA wide-angle seismic reflection transect. Tectonics 34. http://dx.doi.org/10.1002/2014TC00361.

Faccena, C., Piromallo, C., Crespo-Blanc, A., Jolivet, L., Rossetti, F., 2004. Lateral slab deformation and the origin of the western Mediterranean arcs. Tectonics 23 (1). http://dx.doi.org/10.1029/2002TC001488.

Fernandez, M., Marzán, I., Correia, A., Ramalho, E., 1998. Heat flow, heat production, and lithospheric termal regime in the Iberian Peninsula. Tectonophysics 291, 29–53.

Fernàndez, M., Marzán, I., Torne, M., 2004. Lithospheric transition from the Variscan Iberian Massif to the Jurassic oceanic crust of the Central Atlantic. Tectonophysics 386, 97–115. http://dx.doi.org/10.1016/j.tecto.2004.05.005.

Franke, W., 2014. Topography of the Variscan orogen in Europe: failed–not collapsed. Int. J. Earth Sci. (Geol. Rundsch.) 103, 1471–1499. http://dx.doi.org/10.1007/s00531-014-1014-9.

Fullea, J., Fernàndez, M., Zeyen, H., Vergés, J., 2007. A rapid method to map the crustal and lithospheric thickness using elevation, geoid anomaly and thermal analysis. Application to the Gibraltar Arc System, Atlas Mountains and adjacent zones. Tectonophysics 430, 97–117. http://dx.doi.org/10.106/j.tecto.2006.11.003.

Fullea, J., Fernàndez, M., Afonso, J.C., Vergés, J., Zeyen, H., 2010. The structure and evolution of the lithosphere–asthenosphere boundary beneath the Atlantic–Mediterranean transition región. Lithos http://dx.doi.org/10.106/j.lithos.2010.03.003.

Gallart, J., Díaz, J., 2013. Outstanding Moho-depth variations in the Iberian Peninsula, NW Africa and surrounding margins, revealed from controlled-source seismic surveys. 15, EGU2013-5774-1. EGU General Assembly.

Gallastegui, J., 2000. Estructura cortical de la Cordillera y Margen Continental Cantábricos: Perfiles ESCI-N. Trab. Geol. 22, 9–234.

García-Castellanos, D., Fernàndez, M., Torne, M., 2002. Modelling the evolution of the Guadalquivir foreland basin (South Spain). Tectonics 21 (3). http://dx.doi.org/10.1029/2001TC001339.

García-Hernández, M., López-Garrido, A.C., Rivas, P., Sanz de Galdeano, C., Vera, J.A., 1980. Mesozoic palaeogeographic evolution in the External Zones of the Betic Cordillera (Spain). Geol. Mijnb. 59, 155–168.

Gaspar-Escribano, J.M., van Wees, J.D., ter Voorde, M., Cloetingh, S., Roca, E., Cabrera, L., Muñoz, J.A., Ziegler, P.A., Garcia-Castellanos, D., 2001. Three-dimensional flexural modelling of the Ebro Basin (NE Iberia). Geophys. J. Int. 145 (2), 349–368. http://dx.doi.org/10.1029/2003TC001511.

Gomez-Ortiz, D., Agarwal, B.N.P., Thero, R., Ruiz, J., 2011. Crustal structure from gravity signatures in the Iberian Peninsula. GSA Bull. 123 (7–8), 1247–1257. http://dx.doi.org/10.1130/B30224.1.

González-Fernández, A., Torne, M., Córdoba, D., Vidal, N., Matias, L.M., Díaz, J., 1996. Crustal thinning in the southwestern Iberia margin. Geophys. Res. Lett. 23, 2477–2480.

González-Fernández, A., Córdoba, D., Matias, L.M., Torne, M., 2001. Seismic crustal structure in the Gulf of Cadiz (SW Iberian Peninsula). Mar. Geophys. Res. 22, 207–223.

Gueguen, E., Doglioni, C., Fernàndez, M., 1998. On the post-25 Ma geodynamic evolution of the western Mediterranean. Tectonophysics 298, 259–269.

Haxby, W.F., Turcotte, D.L., 1978. On isostatic geoid anomalies. J. Geophys. Res. 83 (B11), 5473–5478. http://dx.doi.org/10.1029/JB080i011p05473.

Jammes, S., Mantschal, G., Lavier, L., Massini, E., 2009. Tectonosedimentary evolution related to extreme crustal thinning ahead of a propagating ocean: example of western Pyrenees. Tectonics 28. http://dx.doi.org/10.1029/2008TC002406.

Jiménez-Díaz, A., Ruiz, J., Villaseca, C., Tejero, R., Capote, R., 2012. The thermal state and strength of the lithosphere in the Spanish Central System and Tajo Basin from crustal heat production and thermal isostasy. J. Geodyn. 58, 29–37.

Jiménez-Munt, I., Fernàndez, M., Saura, E., Vergés, J., Garcia-Castellanos, D., 2012. 3-D lithospheric structure and regional/residual Bouguer anomalies in the Arabia–Eurasia collision (Iran). Geophys. J. Int. 190, 1311–1324.

Julivert, M., Fontboté, J.M., Ribeiro, A. and Conde, L., 1972. Mapa Tectónico de la Península Ibérica y Baleares. E. 1:1.000.000. Inst. Geol. Min. España, Madrid, 113 p.

Lachenbruch, A.H., Morgan, P., 1990. Continental extension, magmatism and elevation; formal relations and rules of thumb. Tectonophysics 174, 39–62.

Lagabrielle, Y., Labaume, P., de Saint Blanquat, M., 2010. Mantle exhumation, crustal denudation, and gravity tectonics during Cretaceous rifting in the Pyrenean realm (SW Europe): insights from the geological setting of the lherzolite bodies. Tectonics 29. http://dx.doi.org/10.1029/2009TC002588.

Larrasoaña, J.C., Parés, J.M., Millán, H., Del-Valle, J., Pueyo, E.L., 2003. Paleomagnetic, structural, and stratigraphic constraints on transverse fault kinematics during basin inversion: the Pamplona Fault (Pyrenees, north Spain). Tectonics 22.

Macquet, M., Paul, A., Pedersen, H.A., Villasenor, A., Chevrot, S., Sylvander, M., Wolyniec, D., 2014. Ambient noise tomography of the Pyrenees and the surrounding regions: inversion for a 3-D Vs model in the presence of a very heterogeneous crust. Geophys. J. Int. 199 (1), 402–415. http://dx.doi.org/10.1093/gji/ggu270.

Mancilla, F., Díaz, J., 2015z. High resolution Moho topography map beneath Iberia and Northern Morrocco from receiver function, analysis. Tectonophysics 663, 419–433.

Martínez-Catalán, J.R., 2011. Are the oroclines of the Variscan belt related to late Variscan strike-slip tectonics? Terra Nova 23, 241–247. http://dx.doi.org/10.1111/j.1365-3121.2011.01005.x.

Martínez-Catalán, J.R., Aller, J., Alonso, J.L., Bastida, F., 2009. The Iberian Variscan orogen. In: García-Cortés, A. (Ed.), Spanish Geological Frameworks and Geosites: An Approach to Spanish Geological Heritage of International Relevance. IGME. ISBN: 978-84-7840-825-2, pp. 13–27.

Mezcua, J., Gil, A., Benarroch, R., 1996. Estudio gravimétrico de la Península Ibérica y Baleares: Madrid. Instituto Geográfico Nacional—IGN (7 pp., 11 Figs).

Muñoz, J.A., 1992. Evolution of a continental collision belt: ECORS-Pyrenees crustal balanced section. In: McClay, K.R. (Ed.), Thrust Tectonics. Chapman and Hall, London, pp. 235–246.

Palomeras, I., Carbonell, R., Flecha, I., Simancas, F., Ayarza, P., Matas, J., Martínez Poyatos, D., Azor, A., González Lodeiro, F., Pérez-Estaún, A., 2009. Nature of the lithosphere across the Variscan orogen of SW Iberia: dense wide-angle seismic reflection data. J. Geophys. Res. 114, B02302. http://dx.doi.org/10.1029/2007JB005050.

Palomeras, I., Carbonell, R., Ayarza, P., Fernàndez, M., Simancas, J.F., Martínez Poyatos, D., González Lodeiro, F., Pérez-Estaún, A., 2011. Geophysical model of the lithosphere across the Variscan Belt of SW-Iberia: multidisciplinary assessment. Tectonophysics 508, 42–51.

Palomeras, I., Thurner, S., Levander, A., Liu, K., Villaseñor, A., Carbonell, R., Harnafi, M., 2014. Finite-frequence Rayleigh wave tomography of the western Mediterranean: mapping its lithospheric structure. G3 15 (1), 140–160. http://dx.doi.org/10.1002/2013GC004861.

Parker, 1972. The rapid calculation of potential anomalies. Geophysics 31, 449–455.

Pavlis, N.K., Holmes, S.A., Kenyon, S.C., Factor, J.K., 2008. An earth gravitational model to degree 2160: EGM2008. 2008 General Assembly of the European Geosciences Union, Vienna, Austria, 2008 April 13–18.

Pedreira, D., Pulgar, J.A., Gallart, J., Díaz, J., 2003. Seismic evidence of Alpine crustal thickening and wedging from the western Pyrenees to the Cantabrian Mountains (north Iberia). J. Geophys. Res. 108 (B4). http://dx.doi.org/10.1029/2001JB001667 (p. ETG 10-1–ETG 10-21).

Pedreira, D., Pulgar, J.A., Gallart, J., Torne, M., 2007. Three-dimensional gravity and magnetic modelling of crustal indentation and wdging in the western Pyrenees–Cantabrian Mountains. J. Geophys. Res. 112, B12405. http://dx.doi.org/10.1029/2007JB005021.

Pedreira, D., Afonso, J.C., Pulgar, J.A., Gallastegui, J., Carballo, A., Fernàndez, M., García-Castellanos, D., Jiménez-Munt, I., Semprich, J., 2015. Geophysical petrological modeling of the lithosphere beneath the Cantabrian Mountains and North-Iberian margin: geodynamic implications. Lithos. http://dx.doi.org/10.1016/j.lithos.2015.04.018 (in press).

Pedrera, A., Marín-Lechado, C., Galindo-Zaldívar, J., García-Lobón, J.L., 2014. Control of preexisting faults and near-surface diapirs on geometry and kinematics of fold-and-thrust belts (Internal Prebetic, Eastern Betic Cordillera). J. Geodyn. 77, 135–148.

Pérez-Estaún, A., Bastida, F., Alonso, J.L., Marquínez, J., Aller, J., Alvarez-Marrón, J., Marcos, A., Pulgar, J.A., 1988. A thin skinned tectonics model for an arcuate fold and thrust belt: the Cantabrian Zone (Variscan Ibero-Armorican Arc). Tectonics 7, 517–537.

Pérez-Estaún, A., Bea, F., Bastida, F., Marcos, A., Martínez-Catalán, J.R., Martínez-Poyatos, D., Arenas, R., Díaz-García, F., Azor, A., Simancas, J.F., González-Lodeiro, F., 2004. La Cordillera Varisca Europea: El Macizo Ibérico. In: Vera, J.A. (Ed.), Geología de España. IGME. ISBN: 84-7840-546-1, pp. 19–228 (881 pp.).

Platt, J.P., Allerton, S., Kirker, A., Mandeville, C., Mayfield, A., Platzman, E.S., Rimi, A., 2003. The ultimate arc: differential displacement, oroclinal bending, and vertical axis rotation in the External Betic–Rif arc. Tectonics 22, 3. http://dx.doi.org/10.1029/2001TC001321.

Popowski, T., Connard, G., French, R., 2005. GMSYS-3D User Guide. Northwest Geophysical Associates, Inc., Corvallis, Oregon (32 pp.).

Riba, O., Jurado, M.J., 1992. Reflexiones sobre la geología de la parte occidental de la Depresión del Ebro. Acta Geol. Hisp. 27, 177–193 (Homenaje a Oriol Riba).

Robert, A.M., Fernàndez, M., Jimenez-Munt, I., Verges, J., 2015. Lithospheric structure in Central Eurasia derived from elevation, geoid anomaly and thermal analysis. In: Brunet, M.F., McCann, T., Sobel, E.R. (Eds.), Geological Evolution of Central Asian Basins and the Tien Shan Range. Geol. Soc. Lond. Spec. Publ., p. 427.

Rodríguez-Fernández, L.R., 2004. Mapa tectónico de España a escala 1:2.000.000. In: Vera, J.A. (Ed.), Geologia de España. SGE-IGME, Madrid.

Root, B.C., van der Wal, W., Novák, P., Ebbing, J., Vermeersen, L.L.A., 2014. Glacial isostatic adjustment in the static gravity field of Fennoscandia. J. Geophys. Res. Solid Earth 120, 503–518. http://dx.doi.org/10.1002/2014JB011508.

Rosenbaum, G., Lister, G.S., Duboz, C., 2002. Reconstruction of the teconic evolution of the western Mediterranean since the Oligocene. In: Rosenbaum, G., Lister, G.S. (Eds.), Reconstruction of the evolution of the Alpine-Himalayan Orogen. J. Virtual Explor. 8, pp. 107–130.

Ruíz, J., Gómez-Ortiz, D., Tejero, R., 2006. Effective elastic thicknesses of the lithosphere in the Central Iberian Peninsula from heat flow: implications for the rheology of the continental lithospheric mantle. J. Geodyn. 41 (5), 500–509.

Simancas, J.F., Ayarza, P., Azor, A., Carbonell, R., Martínez Poyatos, D., Pérez-Estaún, A., González Lodeiro, F., 2013. A seismic geotraverse across the Iberia Variscides: orogenic shortening, collisional magmatism, and orocline development. Tectonics 32, 417–432. http://dx.doi.org/10.1002/tect.20035.

Souriau, A., Granet, M., 1995. A tomographic study of the lithosphere beneath the Pyrenees from local teleseismic data. J. Geophys. Res. 100 (18), 117–118 (134).

Spada, M., Bianchi, I., Kissling, E., Piana Agostinetti, A., Wiemer, S., 2013. Combinign controlled-source seismology and receiver function information to derive 3-D Moho topography for Italy. Geophys. J. Int. 194, 1050–10698. http://dx.doi.org/10.1093/gji/ggt148.

Spakman, W., Wortel, M.J.R., 2004. A tomographic view on western Mediterranean geodynamics. In: Cavazza, W., Roure, F., Spakman, W., Stampfli, G.M., Ziegler, P. (Eds.), The TRANSMED Atlas—the Mediterranean Region from Crust to Mantle. Springer, Berlin Heidelberg, pp. 31–52.

Thurner, S., Palomeras, I., Levander, A., Carbonell, R., Lee, C.-T., 2014. Ongoing lithospheric removal in the western Mediterranean: evidence from Ps receiver functions and thermobarometry of Neogene basalts (PICASSO project). Geochem. Geophys. Geosyst. 15, 1113–1127. http://dx.doi.org/10.1002/2013GC005124.

Torne, M., de Cabissole, B., Bayer, R., Casa, A., Daignières, M., Rivero, A., 1989. Gravity constraints on the deep structure of the Pyrenean belt along the ECORS profile. Tectonophysics 165 (1), 105–116.

Torne, M., Banda, E., García-Dueñas, V., Balanyá, J.C., 1992a. Mantle–lithosphere bodies in the Alboran crustal domain (Ronda peridotites, Betic–Rif orogenic belt). Earth Planet. Sci. Lett. 110, 163–171.

Torne, M., Pascal, G., Buhl, P., Watts, A.B., Mauffret, A., 1992b. Crustal structure of the Valencia Trough (Western Mediterranean). Part 1. A combined refraction/wide angle reflection and near-vertical reflection study. Tectonophysics 203, 1–20.

Torne, M., Fernàndez, M., Comas, M.C., Soto, J.I., 2000. Lithospheric structure beneath the Alboran Basin: results from 3D gravity modeling and tectonic relevance. J. Geophys. Res. 105 (B2), 3209–3228.

Turcotte, D.L., Schubert, G., 2002. Geodynamics: Applications of Quantum Physics to Geological Problems. John Wiley and Sons, New York (450 pp.).

Vacher, P., Souriau, A., 2001. A three-dimensional model of the Pyrenean deep structure based on gravity modelling, seismic images and petrological constraints. Geophys. J. Int. 145, 460–470.

Vera, J.A. (Ed.), 2004. Geología de España. SGE-IGME, Madrid, p. 884 ISBN: 84-7840-546-1.

Vergés, J., 2003. Evolución de los sistemas de rampas oblicuas de los Pirineos meridionales: fallas del Segre y Pamplona. Bol. Geol. Min. Esp. 114, 87–101.

Vergés, J., Fernàndez, M., 2006. Ranges and basins in the Iberian Peninsula: their contribution to the present topography. In: Gee, D.G., Stephenson, R.A. (Eds.), European Lithosphere Dynamics. Geological Society, London, Memoirs 32, pp. 223–234.

Vergés, J., Fernàndez, M., 2012. Tethys–Atlantic interactions long the Iberia-Africa plate boundary: the Betic–Rif orogenic system. Tectonophysics 579, 144–172. http://dx.doi.org/10.1016/j.tecto.2012.08.032.

Vergés, J., Millán, H., Roca, E., Muñoz, J.A., Marzo, M., Cirés, J., Den Bezemer, T., Zoetemeijer, Z., Cloetingh, S., 1995. Eastern Pyrenees and related foreland basins: Pre-, syn- and post-collisional crustal.scale cross-sections. In: Cloetingh, S., Durand, B., Puigdefàbregas, C (Eds.), In Special issue on integrated basin studies. Mar. Petrol. Geol. 12, pp. 903–915.

Vergés, J., Sabat, F., 1999. Constraints on the Neogene Mediterranean kinematic evolution along a 1000 km transect from Iberia to Africa (London). Geol. Soc. 156, 63–80.

Vidal, N., Gallart, J., Dañobeitia, J.J., 1998. A deep crustal seismic transect from the NE Iberian Peninsula to the Western Mediterranean. J. Geophys. Res. 103 (B6), 12381–12396.

Vielzeuf, D., Kornprobst, J., 1984. Crustal splitting and the emplacement of Pyrenean lherzolites and granulites. Earth Planet. Sci. Lett. 67, 87–96.

Vilà, M., Fernàndez, M., Jiménez-Munt, I., 2010. Radiogenic heat production variability of some common lithological groups and its significance to lithospheric thermal modeling. Tectonophysics 490, 152–164. http://dx.doi.org/10.1016/j.tecto.2010.05.003.

Waldhauser, F., Kissling, E., Ansorge, J., Mueller, St., 1998. Three-dimensional interface modelling with two-dimensional seismic data: the Alpine crust–mantle boundary. Geophys. J. Int. 135, 264–278.

Wessel, P., Smith, W.H.F., 1998. New, improved version of Generic Mapping Tools released. Eos. Trans. AGU 79, 579. http://dx.doi.org/10.1029/98EO00426.

Wildi, W., 1983. The orogenic belt of the Rif (Morocco) and the Tell (Algeria, Tunisia) — structure, stratigraphy, paleogeographic and tectonic evolution from Triassic to the Miocene. Rev. Géol. Dynam. Géog. Phys. 24 (3), 201–297.

Zeyen, H.J., Banda, E., Gallart, J., Ansorge, J., 1985. A wide-angle seismic reconnaissance of the crust and upper mantle in the Celtiberian chain (Spain). Earth Planet. Sci. Lett. 75, 393–402.

Ziegler, P.A., 1992. Plate tectonics, plate moving mechanisms and rifting. In: Ziegler, P.A. (Ed.), Geodynamics of Rifting, vol. III. Thematic Discussions. Tectonophysics 215, p. 9.34.